PLOS ONE

RESEARCH ARTICLE

Piperazinyl fragment improves anticancer activity of Triapine

Marta Rejmund[1], Anna Mrozek-Wilczkiewicz[2,3], Katarzyna Malarz[1,3], Monika Pyrkosz-Bulska[1], Kamila Gajcy[1], Mieczyslaw Sajewicz[1], Robert Musiol[1], Jaroslaw Polanski[1]*

1 Institute of Chemistry, University of Silesia, Katowice, Poland, **2** A. Chełkowski Institute of Physics, University of Silesia, Katowice, Poland, **3** Silesian Center for Education and Interdisciplinary Research, University of Silesia, Chorzów, Poland

* jaroslaw.polanski@us.edu.pl

Citation: Rejmund M, Mrozek-Wilczkiewicz A, Malarz K, Pyrkosz-Bulska M, Gajcy K, Sajewicz M, et al. (2018) Piperazinyl fragment improves anticancer activity of Triapine. PLoS ONE 13(4): e0188767. https://doi.org/10.1371/journal.pone.0188767

Editor: Swati Palit Deb, Virginia Commonwealth University, UNITED STATES

Received: June 1, 2017

Accepted: November 13, 2017

Published: April 13, 2018

Data Availability Statement: All relevant data are within the paper and its Supporting Information files.

Funding: The financial support of the National Center of Science grants 2014/13/D/NZ7/00322 (AMW), 2013/09/B/NZ7/00423 (RM) and NCBiR Warsaw ORGANOMET No: PBS2/A5/40/2014 (JP) is greatly appreciated.

Competing interests: The authors have declared that no competing interests exist.

Abstract

A new class of TSCs containing piperazine (piperazinylogs) of Triapine, was designed to fulfill the di-substitution pattern at the TSCs N4 position, which is a crucial prerequisite for the high activity of the previously obtained TSC compounds–DpC and Dp44mT. We tested the important physicochemical characteristics of the novel compounds L^1-L^{12}. The studied ligands are neutral at physiological pH, which allows them to permeate cell membranes and bind cellular Fe pools more readily than less lipid-soluble ligands, e.g. DFO. The selectivity and anti-cancer activity of the novel TSCs were examined in a variety of cancer cell types. In general, the novel compounds demonstrated the greatest promise as anti-cancer agents with both a potent and selective anti-proliferative activity. We investigated the mechanism of action more deeply, and revealed that studied compounds inhibit the cell cycle (G1/S phase). Additionally we detected apoptosis, which is dependent on cell line's specific genetic profile. Accordingly, structure-activity relationship studies suggest that the combination of the piperazine ring with Triapine allows potent and selective anticancer chelators that warrant further *in vivo* examination to be identified. Significantly, this study proved the importance of the di-substitution pattern of the amine N4 function.

Introduction

Thiosemicarbazones (TSCs) have a broad range of biological activity including antitumor, antimalarial and antimicrobial activity [1], and therefore, for many years, studies of α-(N)-heterocyclic TSCs have been attracting considerable interest. In particular, the antitumor properties of 2-formylpyridine thiosemicarbazone were reported over 50 years ago [2]. With regard to potential pharmaceutical applications, Triapine (3-aminopyridine-2-carboxaldehyde thiosemicarbazone; 3-AP) is the most prominent representative of this class, as it has already been investigated in more than 30 clinical phase I/II trials [3–10]. Moreover, di-2-pyridylketone-4-cyclohexyl-4methyl-3-thiosemicarbazone (DpC) is currently entering clinical phase I studies as a potential anticancer agent. Although clinical studies have concluded that Triapine revealed activity against hematological cancer types (e.g. advanced leukemia [8,11]), it also showed

disappointing results against a variety of solid tumor types such as advanced adenocarcinoma of the pancreas [12], non-small-cell lung cancer [3] and renal cell carcinoma [13]. Furthermore, some side effects include the formation of methemoglobin and hypoxia [3,8,9], which were observed after administration. Therefore, the development of new Triapine analogs with a potent anticancer activity would be significant.

The broad range of the biological activity of TSCs corresponds to their versatile binding modes with the transition and main group metal ions [14]. Moreover, it has been observed that, generally, the biological activity of the complexes of TSCs is often higher than that of corresponding metal-free ligands. To gain further insight into the coordination chemistry of TSCs, thermodynamic data such as the stability constants of metal complexes, which help in optimizing the chemical or biological properties that are essential for potential medicinal applications, are needed. In particular, copper complexes have a considerably higher anticancer activity than the uncomplexed ligands that also have lower IC_{50} values against cancer cells than other described topoisomerase-II inhibitors [15]. In contrast, Triapine complexation to iron resulted in the reduced cytotoxicity compared to the metal free ligand.

Although Triapine, similar to the recently developed Dp44mT (di-2-pyridylketone-4,4-dimethyl-3-thiosemicarbazone), has been evaluated as a potential anticancer agent, the molecular mechanisms of its action have not been fully elucidated. Several paradigms have been proposed to explain the activity of these compounds [16,17] including blocking cellular iron uptake from transferrin [18]; mobilizing iron from cells; inhibiting ribonucleotide reductase, the iron-containing enzyme that is involved in the rate-limiting step of DNA synthesis [19] or forming reactive oxygen species (ROS) [20]. The effect of metal chelation suggested among potential determinants of the mechanism origins are among the most important determiners deciding that the mechanism(s) of action of these compounds are incompletely understood.

In this research, we designed and obtained new Triapine analogs for the first time through incorporating the piperazine ring as a promising new pharmacophore group to replace the N terminal amino group (Fig 1). While the substitution pattern at the N4 atom of TSCs appears to be critical for the activity of Dp44mT, there were no similar studies for Triapine. Therefore, we tested di-substitution at the N4 atom by constructing an N4-based piperazine, which is a fragment that is present in several active TSCs [21–23]. First, we hoped that this could modulate the antiproliferative activity of the new analogs because the piperazine heterocycle is found in a wide variety of biologically active compounds, some of which are currently being used in clinical therapy [24–27]. In particular, new derivatives could have a significant impact on pharmacokinetics and pharmacodynamics, while the replacement of the unsubstituted NH_2 function with the piperazine fragment should increase the lipophilicity of the new analogs. Second, the modification of the substitution pattern of piperazine is a standard drug design scheme that has often resulted in an increased medicinal potential of the analogs [28].

Accordingly, we describe the synthesis of a series of new N4- piperazinylogs of Triapine that were tested for their anticancer activity vs. a broad spectrum of cancer cell lines. As the metal complexation of the piperazine ring has been reported as an important issue in the biological activity for these compounds [29,30], we tested L^1-L^{12} as potential chelators for transition metals. Solution equilibria of the all the ligands and their copper(II) and iron(III) complexes were studied using UV-Vis titration.

Results and discussion

Chemistry

Design and synthesis. Identifying the functional fragments for drug design is a complex problem that involves different approaches including those that have an experimental and

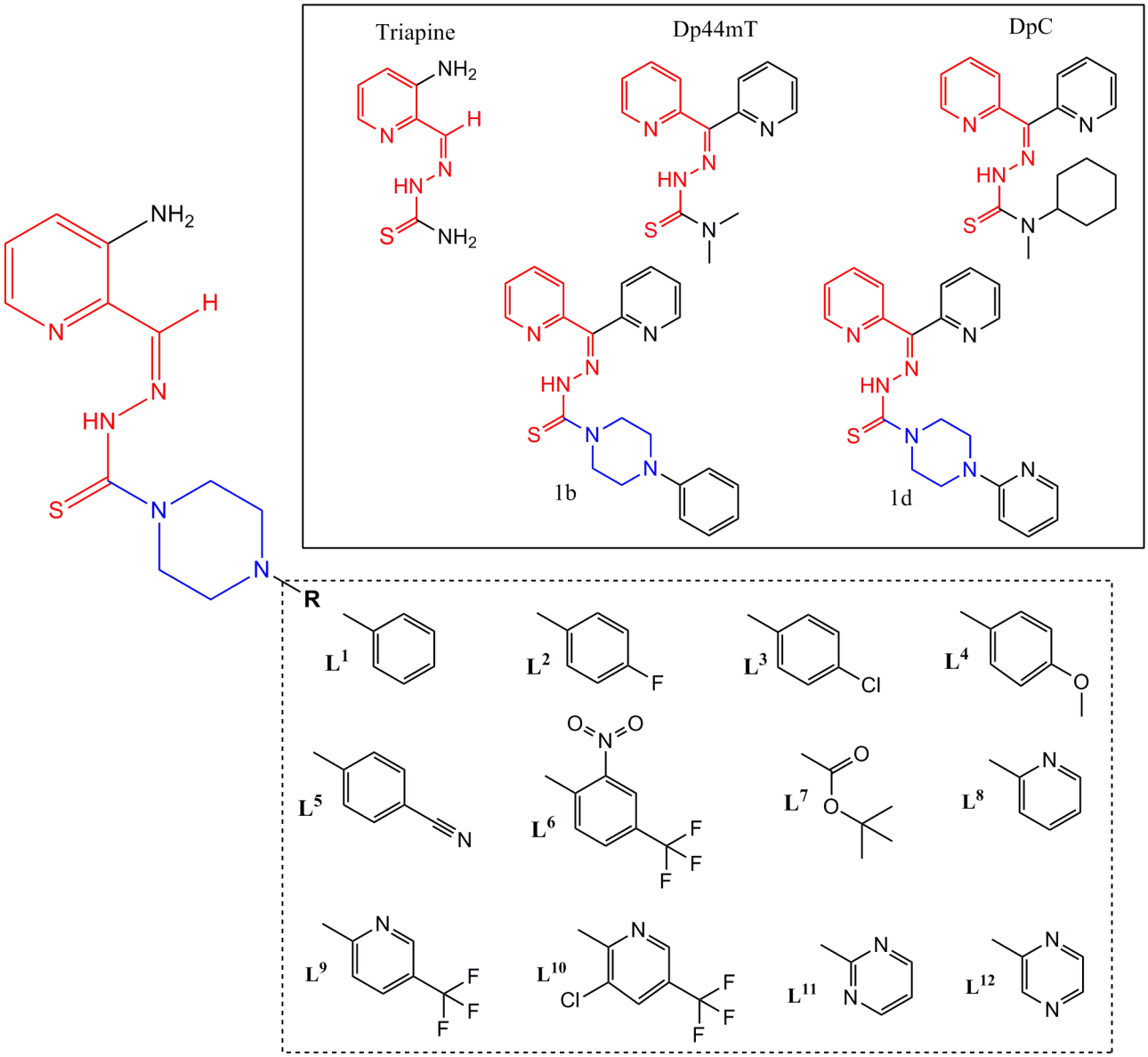

Fig 1. Design strategy for novel TSCs (L^1-L^{12}). All designed ligands are based on the Triapine skeleton, which is present in the active analogs Dp44mT, DpC and 1b, 1d that have been described as highly active analogs [21].

https://doi.org/10.1371/journal.pone.0188767.g001

theoretical basis. The latter consist of a variety of methods, among which are those to identify advantageous sub-structures, scaffolds and/or linkers on the basis of previously reported compounds. Alternatively, the fragmentation of organic molecules into smaller moieties is an important method in retrosynthetic analysis and has inspired various pseudo-retrosynthetic approaches [31]. This has identified fragments that may be useful for drug design. For example, the di-2-pyridyl [32–35], quinolinyl [36], piperazinyl [37,38], morpholinyl [39] and quinoxalinyl [40] motifs, which are common fragments in other anti-cancer agents, have been incorporated into the design of the novel TSCs reported herein (Fig 1).

We have previously examined a variety of TSCs that demonstrate *in vitro* anti-proliferative activity [21,41,42]. Earlier studies indicated that di-substitution at the terminal (N4) nitrogen

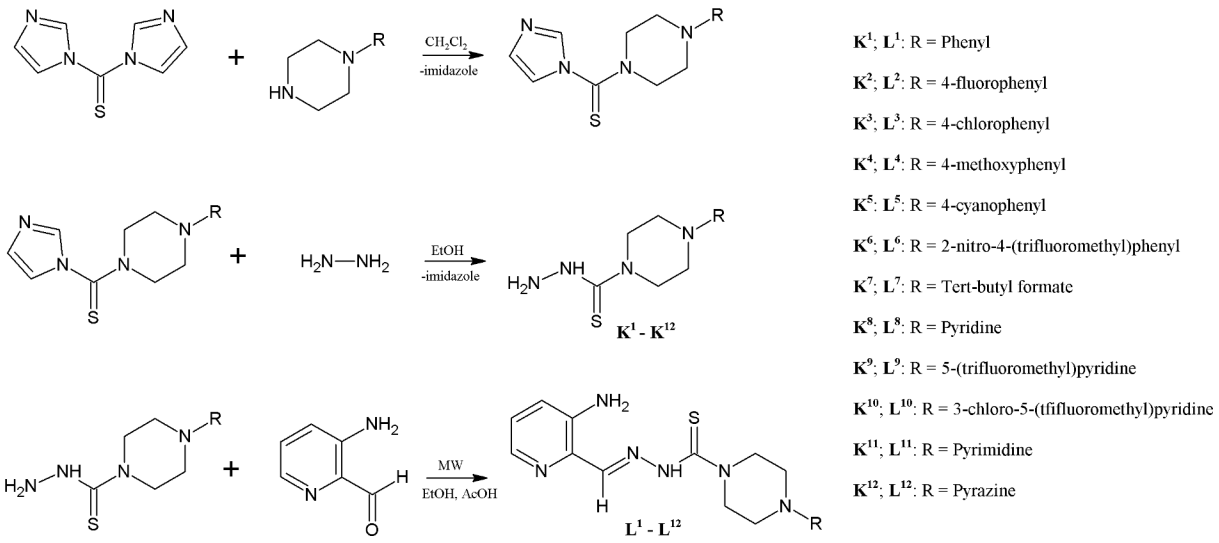

Fig 2. Synthesis of the thiosemicarbazides K^1-K^{12} and thiosemicarbazones L^1-L^{12}.

https://doi.org/10.1371/journal.pone.0188767.g002

is crucial for effective anti-cancer activity [21,32,34,42]. Therefore, in the present study, we transformed the amine function in the southern part of the Triapine molecule into the form of a piperazine ring. This formed a di-substitution at the N4 position that was discovered to be of crucial importance for the activity of DpC and Dp44mT, which has never been tested for Triapine. In particular, there is a fragment that is present in several active TSCs in this piperazine ring [23,43].

The synthetic protocol that was used to produce the target molecules is outlined in Fig 2. The precursors that are required to obtain the desired Triapine derivatives, the thiosemicarbazides K^1-K^{12}, were synthesized from commercially available reagents in a two-step process that mostly produced high yields (69–98%). The treatment of (1,1'-thiocarbonyl)bis-1H-imidazole with the appropriate derivative of piperazine, followed by the reaction with hydrazine hydrate, produced the N-substituted piperazine-based thiosemicarbazides in a high yield. The final TSC series, L^1-L^{12} (Fig 2), were synthesized in a moderate to high yield (20–83%) using the Schiff-based condensation of the 3-aminopyridine-2-carboxaldehyde with the prepared thiosemicarbazides K^1-K^{12} in a microwave reactor, which produced novel Triapine-based ligands after crystallization with methanol. All the synthesized compounds were confirmed using ^{1}H, ^{13}C NMR and MS spectroscopic techniques.

Chelating properties

Protonation constants of the Triapine-derivative ligands. Spectrophotometric titrations were performed in order to probe the acid-based equilibria that were associated with each ligand and to determine the pH range over which the chelator was in its charge neutral form. This property is important in understanding the passage of a molecule through the cell membranes, as charged chelators have poor access [33,44]. These studies were performed in an 80% (w/w) MeOH/H_2O solvent mixture due to the low solubility of these compounds in pure water. The fully protonated forms of the ligands have four L^1-L^7 or five L^8-L^{12} dissociable protons, respectively. All the studied ligands possess one dissociable proton at the hydrazanic group of the thiosemicarbazone moiety, one at pyridine ring and two at the piperazine moiety. An additional proton in L^8-L^{12} derives from the additional pyridine, pyrimidine or pyrazine ring, respectively; however, not all of them could be determined under these experimental

conditions. The protonation constants that were obtained are given in Table 1 and the species distribution diagram of the protonated species of the selected ligand is presented in Fig 3.

The UV/Vis spectrophotometric titrations revealed characteristic spectral changes in the 240–450 nm wavelength range. All studied ligands displayed intense absorption bands in this range, which were dependent on the protonated state of the molecule. The bands with a maximum absorption $\lambda_{max} \approx$ 380 nm-404 nm were assigned to the n→π* transitions of the pyridine ring. The less intense bands at ≈ 290 nm originated mainly from the π→π* transitions of the azomethine chromophore [45–47]. During the first deprotonation step ($[H_3L]^{2+} \rightarrow [H_2L]^{+}$, we observed a blueshift and a decrease in the intensity of the absorption maximum in the visible region. The next two deprotonation steps were accompanied by a redshift and an increase in intensity (Fig 1B and S1 Fig). Following the deprotonation of the N^2-H group, the negative charge is transferred mainly to the S atom via the thione-thiol tautomeric equilibrium.

The proton dissociation constants and the spectra of the individual ligand species (Table 1) were calculated based on the deconvolution of the pH-dependent UV-Vis spectra. The obtained logK_a values are in a reasonably good agreement with previously reported thiosemicarbazones ligands [45–47]. The concentration distribution curves, together with the electronic spectra as a function of pH, are reported in the Supporting Information (S1 Fig).

For the studied ligands, the first protonation constant corresponded to the protonation of the hydrazanic = N-NH group. A decreased value, about one order of magnitude lower than in the other reported *N*-pyridyl thiosemicarbazones ligands (log$K \sim$ 10.2–11), can most probably be attributed to the substitution of the piperazine ring by an aromatic ring (L^1-L^7), pyridine (L^8-L^{10}) or the pyrimidine and pyrazine moiety in L^{11} and L^{12}, respectively. This effect is the result of the electron-withdrawing effect of these substituents. On other hand, the hydrogen bond between the pyridyl nitrogen and the = N-NH hydrazanic moiety is most probably responsible for the marked differences in the value of log*K*. The next protonation constant, log*K* with a value of 5.7–7.2 was assigned to the piperazine moiety. The obtained values of log*K* of the piperazine functional group of the studied ligands are comparable to the reported

Table 1. Protonation constants (logβ^{H}) of the L^1-L^{12} ligands in the MeOH/H_2O mixed solution[a].

	$\log\beta_1^H$	$\log\beta_2^H$	$\log\beta_3^H$	$\log\beta_4^H$	**logK_1**	**logK_2**	**logK_3**	**logK_4**
L^1	9.67(1)	16.17(1)	19.49(1)		9.67	6.50	3.32	
L^2	9.73 (1)	15.40 (2)	18.70(2)		9.73	5.77	3.20	
L^3	9.25(1)	15. 83(2)	19.05(2)		9.25	6.58	3.22	
L^4	9.58(1)	13.35(2)	19.76(3)		9.58	6.77	3.41	
L^5	9.47(1)	15.15(2)	18.31(2)		9.47	5.68	3.16	
L^6	9.43(1)	15.65(1)	18.91(1)		9.43	6.22	3.26	
L^7	9.94(1)	16.93(2)	20.21(3)		9.94	6.99	3.28	
L^8	9.96(1)	17.34 (1)	22.07(3)	25.39(3)	9.96	7.38	4.73	3.32
L^9	9.70 (1)	17.26 (2)	22.41(4)	25.58(4)	9.70	7.56	5.15	3.17
L^{10}	9.66 (1)	17.23 (1)	22.74(2)	25.96(3)	9.66	7.57	5.51	3.22
L^{11}	9.55(1)	15.93 (2)	19.33(2)		9.55	6.38	3.40	
L^{12}	9.63 (1)	16.37 (2)	19.60(2)		9.63	6.74	3.23	
Triapine	10.64 (1)	14.12 (1)			10.64	3.48		
Triapine	10.86 (1)[45]	14.65 (1)[45]			10.86	3.79		

[a] Solvent MeOH/H_2O 80/20 by weight

I = 0.1 M KCl, T = 25.0˚C. The reported errors on logβ are given as 1σ.

https://doi.org/10.1371/journal.pone.0188767.t001

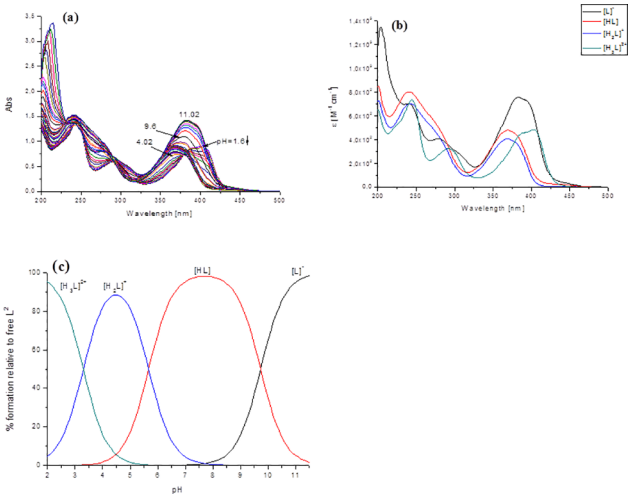

Fig 3. (a) Absorption spectrophotometric titration vs. pH of the free L^2 ligand; (b) electronic spectra of the protonated species of L^2; (c) concentration distribution curves for the L^2 species. (I = 0.1 M (KCl) in 80% (w/w) MeOH/H_2O; T = 25.0˚C; [L^2] = 5x10^{-5}M; pH 1.6–11.02).

https://doi.org/10.1371/journal.pone.0188767.g003

values [48–50] or log*K* values determined for the other TSC-based hybrids, mPip-FTSC and mPip-dm-FTSC (log*K* 7.28) [46]. The log*K* with value 3.1–3.4 can presumable be attributed to protonation of the pyridinium nitrogen. These values are in good agreement with the most popular TSC as is Triapine and other published *α-N-* pyridyl thiosemicarbazones [45,51]. For ligands L^8-L^{10} were observed additional log*K* with value 4.73; 5.15 and 5.51 respectively. These values most probably corresponded to protonation of additional pyridinium unit, which is in agreement with the tabulated log*K* values of pyridine (5.23) [52].

The next acidic logK_s occurred well below pH 2.5 and the constants corresponding to these processes were not determined under the experimental conditions used in this study.

It should be noted that all of the measured log*K*s are macroscopic constants and that further constants cannot be ascribed to the protonation of either of the donor groups without detailed NMR titrations of the ligand [53]. However, taking into account the solvent conditions (*vide supra*) and comparing the observed data with those of a series of previously investigated ligands [45,46], the basicity of the substituents included in the studied ligand most probably follows the trend–hydrazine N^2H group > piperazine > additional function group (e.g. pyridine, pyrimidine or pyrazine) ≈ pyridine.

For the studied ligands, the neutral uncharged form dominated at a physiological pH of 7–8.5, thus enabling a facile passage across the cell membranes. This would explain, at least in part, the high biological activity of these chelators by mobilizing intracellular Fe; preventing Fe uptake from the serum Fe transport protein, transferrin (Tf) and also inhibiting cellular proliferation [20]. The protonated form (Fig 3) became dominant below pH 5, while the deprotonated form was only important above pH 11 (Fig 3 and S1 Fig). Hence, if these agents are ever given as drugs via the oral route, the low pH of the stomach (pH 1–2) would prevent the absorption of the drug as the molecule would be charged [54]. More facile absorption would occur in the small intestine where the higher pH (pH 5–7) would result in a neutral ligand and a greater uptake [54].

Ability to chelate Cu(II) and Fe(III). To evaluate the complex formation ability for the studied Triapine-derivative ligands, we performed the spectroscopic titration of the solutions of all the L^1-L^{12} compounds with copper and iron ions. We titrated the studied ligands with the above-mentioned metal ions to generate their metal-complexes *in situ* at the following

metal to ligand ratios 1:1–1:5. The isosbestic curves for the selected ligands are presented in Fig 4.

In general, the addition of a metal ion to the ligand solution caused distinguishable changes in the visible region of the ligand spectra. This behavior suggests an instantaneous complex formation in the solution from the reaction of each of the studied ligands with the metal ions used. All the ligands displayed the characteristic intense transitions in the range 400–500 nm

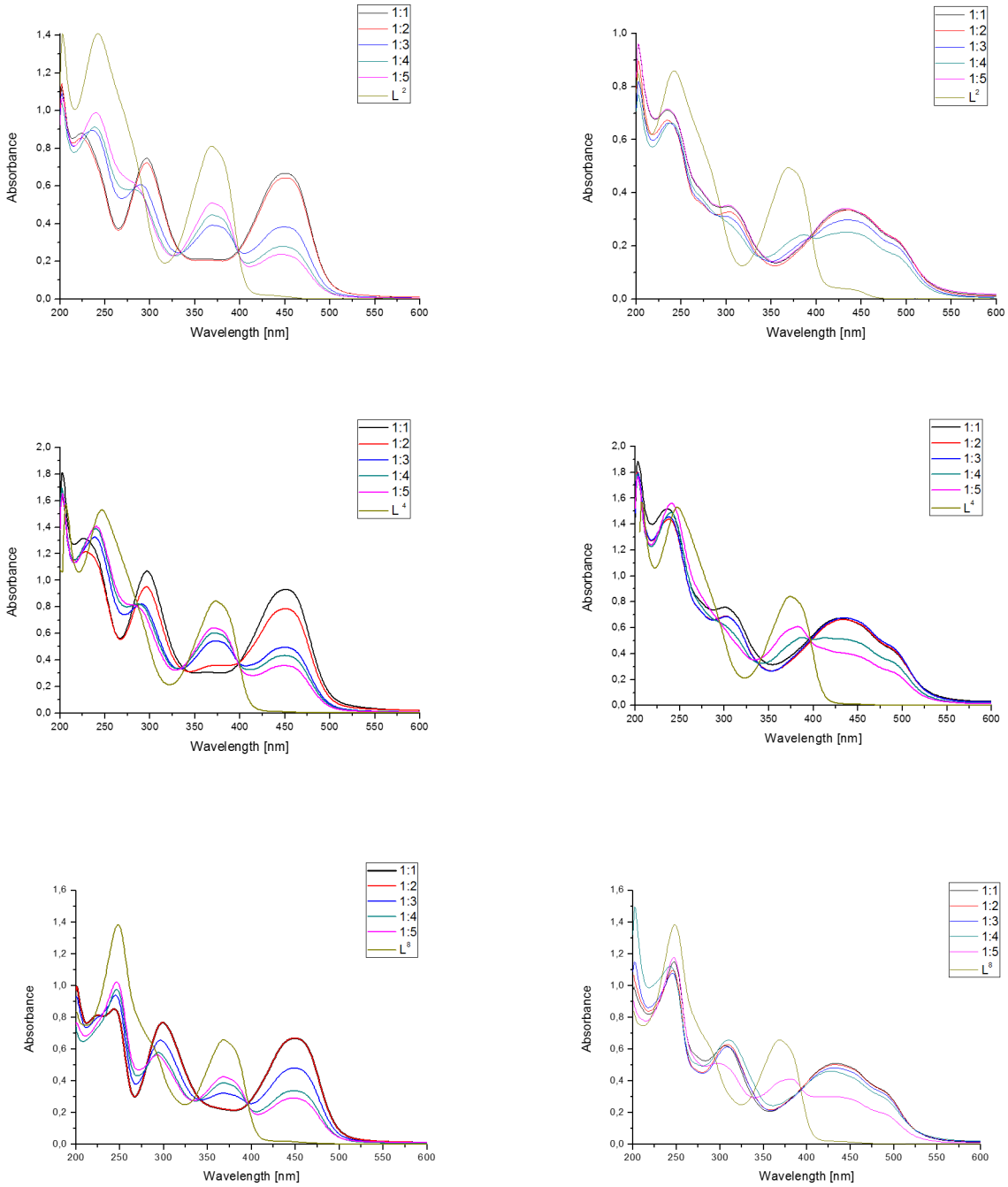

Fig 4. Electronic absorption spectra of the Cu(II) and Fe(III)-L^2; L^4; L^8 system recorded at various metal to ligand ratios. I = 0.1 M (KCl) in 80% (w/w) MeOH/H_2O; T = 25.0˚C; [L] = 5x10^{-5}M.

https://doi.org/10.1371/journal.pone.0188767.g004

for Cu(II) and 380–510 nm for Fe(III) that spanned into the visible region. Fig 4 shows the electronic spectral change that was observed in the MeOH/H_2O 80/20 w/w solution when Cu (II) or Fe(III) was added to the selected ligands L^2, L^4 and L^8. In the absence of metal ions, the light yellow solution showed intensive absorption bands at $\lambda_{max} \approx 250$ nm, $\lambda_{max} \approx 290$ nm and $\lambda_{max} \approx 380$ nm—404 nm. As the Cu(II) or Fe(III) ion solution was added, the signals of the ligand alone decreased and those of the complexes increased in intensity at 430–450 nm with some isosbestic points at ≈ 337 nm and 395 nm (S1 Table). The presence of this band indicates a LMCT (*ligand to metal charge transfer*), which is typical of the Cu(II) L complex. This transition band corresponds to the S→Cu(II) and N_{py}→Cu(II) transition. Similar ligand to metal charge transfer bands have also been observed in the complexes of other TSC ligands [45,46,51]. No d-d bands were observed due to the low concentration (~ 10^{-5}M range) of the Cu(II) complexes in the solution. These bands should have a low intensity in the region of 600–700 nm.

In the studied ligands, the formation of mono complexes for Fe(III) resulted in a shoulder in the interval 450–620 nm. As metal-free ligands do not absorb in this region, these are most probably charge-transfer (CT) bands of the Fe-L complexes [46,51]. Additionally, we developed the characteristic CT bands $\lambda_{max} \approx 639$ nm of the Fe(III)-L complexes in the wavelength of 580–680 nm, which was also detected in the other Fe(III)-TSC systems [46,51]. In conclusion, the analysis of the results showed that the presented ligands can act as effective copper or iron chelators.

Anticancer activity

Cytotoxicity of novel Triapine analogs. All the newly synthesized compounds were evaluated against a panel of cancer and normal cell lines for their cytotoxic activity (Table 2). Among the cancer cells, we analyzed the cytotoxicity of the tested compounds against colon cancer with a normal (HCT116 $p53^{+/+}$) and deleted TP53 suppressor gene (HCT116 $p53^{-/-}$), which encodes the p53 protein. This was designed to allow the assayed activities to be compared with the literature data as a number of previous reports on the antiproliferative potency of TSCs presented results from these cells [21,41,42,55–58]. Moreover, colon cancers are among those that are particularly associated with a higher iron uptake and metabolism [59,60].

Table 2. Anti-proliferative activity (IC_{50} values) of the novel Triapine analogs compared to Triapine in several tumor cell-types and normal human dermal fibroblast (NHDF) cells. Individual IC50 values IC50 < 1μM, IC50 1–10 μM, IC50 > 10 μM are coded by red, yellow and grey, respectively.

Name	IC_{50} [μM]					
	HCT116 $p53^{+/+}$	HCT116 $p53^{-/-}$	MCF-7	U-251	Hs683	NHDF
L^1	1.524 ± 0.445	0.128 ± 0.012	0.532 ± 0.145	0.403 ± 0.090	1.436 ± 0.358	>25
L^2	0.526 ± 0.077	0.152 ± 0.074	0.360 ± 0.111	0.887 ± 0.158	2.487 ± 0.512	>25
L^3	0.120 ± 0.005	0.167 ± 0.018	0.204 ± 0.049	0.128 ± 0.012	1.483 ± 0.335	>25
L^4	1.328 ± 0.209	0.185 ± 0.088	0.424 ± 0.149	0.649 ± 0.170	4.457 ± 0.954	>25
L^5	1.450 ± 0.452	0.7461 ± 0.354	3.807 ± 1.023	2.569 ± 0.675	10.050 ± 2.643	>25
L^6	0.139 ± 0.016	0.270 ± 0.007	0.470 ± 0.097	0.381 ± 0.042	1.894 ± 0.812	>25
L^7	0.762 ± 0.238	1.133 ± 0.049	2.536 ± 0.400	3.084 ± 1.273	4.624 ± 1.031	>25
L^8	1.900 ± 0.292	0.139 ± 0.020	1.120 ± 0.113	1.070 ± 0.280	1.162 ± 0.307	>25
L^9	0.422 ± 0.113	0.123 ± 0.061	0.204 ± 0.024	0.277 ± 0.058	0.844 ± 0.238	>25
L^{10}	0.170 ± 0.015	0.159 ± 0.011	0.258 ± 0.040	0.137 ± 0.016	0.195 ± 0.021	>25
L^{11}	0.668 ± 0.045	0.650 ± 0.055	1.730 ± 0.388	1.268 ± 0.374	2.838 ± 0.581	>25
L^{12}	0.435 ± 0.108	0.342 ± 0.042	2.218 ± 0.638	0.743 ± 0.109	2.595 ± 0.237	>25
L^{13}/3-AP	1.121 ± 0.277	1.336 ± 0.338	2.328 ± 0.431	1.476 ± 0.558	1.763 ± 0.292	>25

https://doi.org/10.1371/journal.pone.0188767.t002

This makes them potentially vulnerable to treatments that target iron homeostasis. We also tested the cell lines of the brain tumor (U-251, Hs683) and breast cancer (MCF-7) cell lines. Breast cancers are among the most frequent cancers and their aggressiveness and treatment prognosis is strongly connected with iron metabolism [61–63]. Namely, it has been confirmed that the regulation pattern of the iron regulatory genes determined the metastasis potency and may be used as a predictive factor in the therapeutic strategy planning [62,64]. Glioblastomas, on the other hand, are one of the most dangerous cancers because no effective therapeutic regimes exist to treat them. The prognoses in these types of cancer are generally poor and the mean survival time does not exceed two years even under combination therapy [65,66]. Interestingly, those cancers also express an altered metabolism of iron and remain susceptible to treatments with iron chelators [67]. Both desferioxamine (DFO) and deferiprone have shown promising results in the U-251 cell line [68]. However, despite these encouraging promises, there are very few reports concerning the activity of TSCs in glioblastomas. Importantly, for the compounds to be useful as anti-cancer drugs, the selectivity between the tumor cells and normal, mortal cell types must be revealed. Therefore, we additionally tested the new compounds on the NHDF cell line. In general, all the examined analogs showed a significantly higher anti-proliferative activity than the reference Triapine. The most active compound was compound L^3 with an IC_{50} value equal to 0.12 μM in the HCT116 $p53^{+/+}$ cell line. The activity of this compound was very similar for all the cancer lines and fluctuated around 0.12–0.2 μM. This derivative also has a promising therapeutic index (208 in HCT116 $p53^{+/+}$ see S2 Table) as its cytotoxicity against normal cell lines is relatively low. However, the glioma cell line Hs683 is an exception here as it has an IC_{50} with a ten-fold higher value for L^3. In fact, the glioblastoma Hs683 exhibited resistance to almost all the tested analogs except for the L^9 and L^{10} derivatives. Those two analogs were active against all the tested cancer cell lines. In general, ligands that are halogenated at the terminal aromatic ring exerted a higher activity than their unsubstituted non-halogenated counterparts (compare L^1 vs. L^2, L^3). The compounds with diazine rings appeared to be less active than phenol (L^1 vs. L^{11} and L^{12}) and the pyridine ring produced a derivative that was even less active (L^8). This may have been the result of the unfavorable p*Ka* of the molecule and is in contrast with previous reports [21]. The trifluoromethyl substitution was very active against all the cancer cell lines that were tested. It also appeared to be less toxic against normal fibroblasts (L^6, L^9, L^{10}).

The effect of the TP53 status on a cell's susceptibility to the some of the Triapine analogs is interesting. The derivatives L^1, L^4, L^5 and L^8 were approximately 2–14 times more effective against HCT116 ($p53^{-/-}$) than against the wild-type cells. In turn, this scheme was inverted for compound L^7, which exhibited a reversed effect, as these compounds appeared to be slightly less active against the $p53^{-/-}$ cell line. In addition to these observations, the colon cancer cells, breast and U-251 glioma appeared to be similarly susceptible to TSCs. A particularly interesting exception was the Hs683 cell line, which appeared to be relatively resistant to almost all of the compounds with a ten-fold higher mean IC_{50}. This phenomenon is important when considering the similar origin of the U-251 and Hs683 lines (from a malignant glioblastoma tumor and from a glioma lesion of 75-year-old Caucasian male patient, respectively). The explanation probably lies in a different level of the basal iron homeostasis, e.g. originating from the different activity and concentration of the transferrin (Tf) receptors. It has previously been reported that Hs683 is significantly more resistant than U-251 to Tf-toxins such as the pokeweed antiviral protein, momordin or gelonin [69]. This suggests that in resistant cells, the cellular metabolism of iron can be restored more easily.

To summarize, the novel compounds demonstrated the greatest promise as anti-cancer agents with both a potent and selective anti-proliferative activity (Table 2). Accordingly, the structure-activity relationship reveals that the combination of the piperazine ring with

Triapine allows potent and selective anticancer chelators that warrant further *in vivo* examination to be identified. In particular, the compounds L^9 and L^{10}, which have fluorine atoms, appeared to have the best activity against all of the cancer lines that were tested. For this reason, we selected L^9 for a more thorough investigation of the molecular mechanisms of its activity.

Cell cycle analysis. The results presented in Fig 5 illustrate the effects of L^9, which is one of the most active TSCs of the current series, on the regulation of the cell cycle in the HCT116 $p53^{+/+}$, U-251 and MCF-7 cell lines. In general, we observed a decrease in the percentage of cells in the G0/G1 phase 24 h after treatment with L^9 in all the cell lines. This effect was especially strong in the U-251 cells, in which L^9 decreased the cell count in the G0/G1 phase to 50% compared to the untreated cells (78%) (Fig 5B). Additionally, the L^9 compound induced an increase in the percentage of cells in the S phase in all of the tested cell lines. The strongest

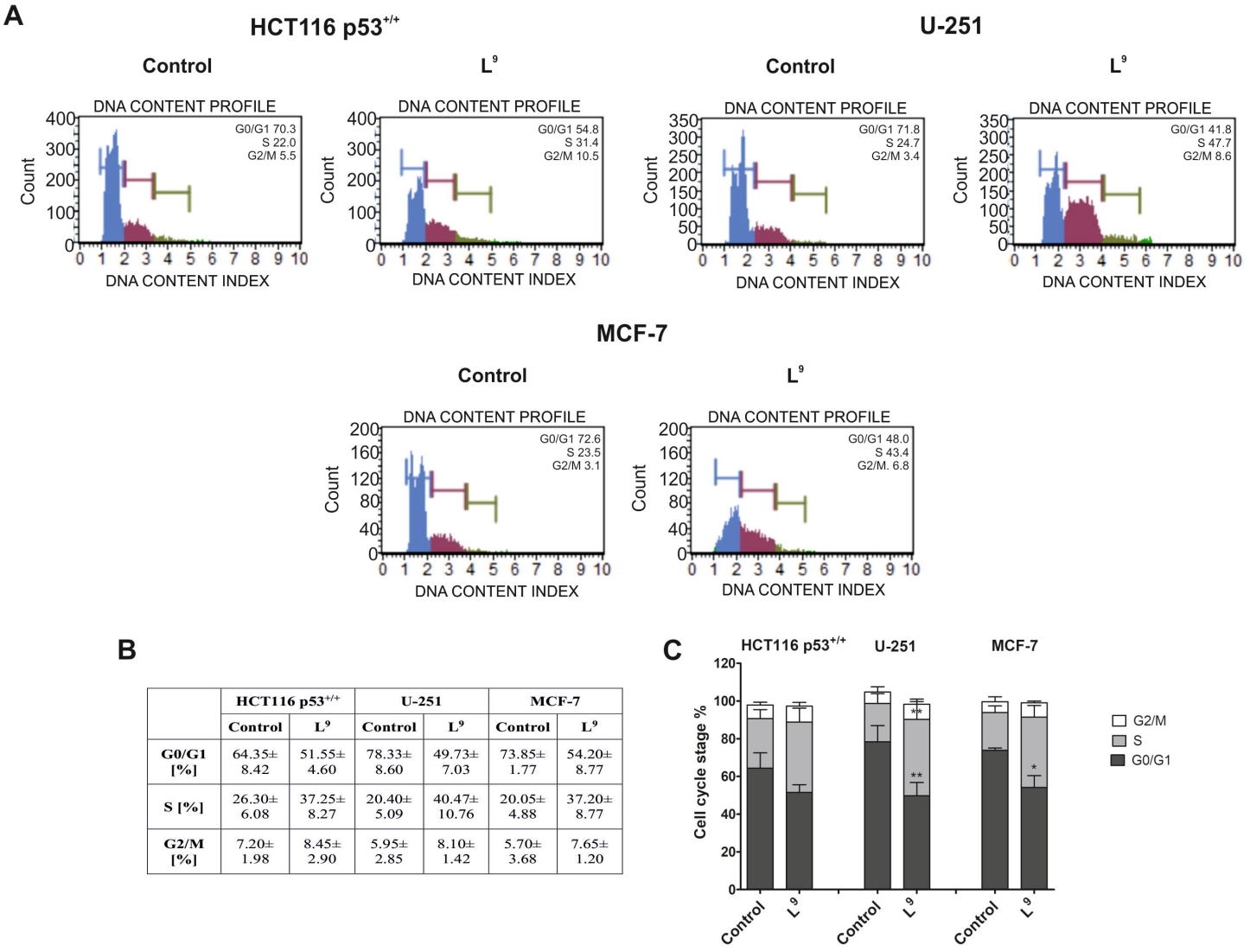

	HCT116 $p53^{+/+}$		U-251		MCF-7	
	Control	L^9	Control	L^9	Control	L^9
G0/G1 [%]	64.35± 8.42	51.55± 4.60	78.33± 8.60	49.73± 7.03	73.85± 1.77	54.20± 8.77
S [%]	26.30± 6.08	37.25± 8.27	20.40± 5.09	40.47± 10.76	20.05± 4.88	37.20± 8.77
G2/M [%]	7.20± 1.98	8.45± 2.90	5.95± 2.85	8.10± 1.42	5.70± 3.68	7.65± 1.20

Fig 5. Influence of L^9 on the regulation of the cell cycle in the HCT116 $p53^{+/+}$, U-251 and MCF-7 cells. The histograms show the percentage of cells in the G0/G1, S and G2/M phases of the cell cycle for one of the experiments (A). The table shows the mean ± SD percentage of the cells in the G0/G1, S and G2/M phases of the cell cycle from three independent experiments (B). Data were analyzed using one-way ANOVA with Bonferroni's post-hoc test: $^{*}p<0.05$, $^{**}p<0.01$, $^{***}p<0.001$ compared to the control (**C**).

https://doi.org/10.1371/journal.pone.0188767.g005

effect was observed for U-251 (41%). Moreover, 24 h after treatment with L^9, we did not observe any changes in the percentage of cells in the G2/M phase compared to the untreated control. These results suggest that the tested TSCs may induce the arrest of the cell cycle in the G1/S phase, thus contributing to the induction of cell death. This result is in good agreement with literature data for TSC [70,71] as well as iron chelator in general [72–74]].

Analysis of programmed cell death–annexin V-FITC assay. The ability of L^9 to induce apoptosis in the HCT116, U-251 and MCF-7 cells was determined using Annexin V-FITC staining. The results are presented in Fig 6. The largest percentage of apoptotic cells was observed in the MCF-7 cell line. In this case, we detected a six-fold increase in the number of dead cells (compared to the untreated cells). The total apoptotic value was 55% (Fig 6B). For HCT116 $p53^{+/+}$, we also noticed a four-fold increase in the number of dead cells. The situation was different for the U-251 cell line, in which the percentage of total apoptotic cells was three times higher in L^9-treated cells than the control. All observed changes are statistically significant.

Western blot analysis of the cell cycle and cell death proteins. Alterations in the iron level are associated with the progression of the cell cycle. Due to their ability to bind with cellular iron, iron chelators may affect the expression of many proteins that are responsible for controlling the cell cycle. The most important regulators of the cell cycle are cyclins, cyclin-dependent kinases (cdks), p53 and cyclin-dependent kinase inhibitors such as p21 [73]. The cdks are dependent on the cyclins to modulate their phosphorylation activity, and therefore the activity of the cyclin-cdk complexes are affected by the cyclin-dependent kinase inhibitors. The progression through the G1 phase and then transition to the S phase of the cell cycle are controlled in part by the activation of the cyclin D1/cdk4 and cyclin E/cdk2 complexes [74]. Additionally, the activity of cyclin D1 is associated with the p21 protein, which plays a crucial role in triggering various effects on cell cycle regulation. Thus, a decrease in the expression of the $p21^{CIP1/WAF1}$ protein may lead to the arrest of the cell cycle in the G1/S phase since this protein can stabilize the cyclin D1-cdk complexes [75,76]. On the other hand, the effect of iron chelation may up-regulate $p21^{CIP1/WAF1}$, which may induce the signaling pathways, thus leading to apoptosis [74,77]. In turn, the cdc2 protein, which is the catalytic subunit that complexes cyclin A, B, is responsible for the transition into the G2/M phase of the cell cycle [74,77]. With this in mind, we evaluated the impact of L^9, as well as reference 3-AP, on the expression of cyclin E, p21 and the cdc2 proteins in HCT116 $p53^{+/+}$, U-251 and MCF-7 cells. As is presented in Fig 7, we observed various patterns of the expression of the cell cycle proteins in the investigated cell lines. Treatment with L^9 led to a slight increase in the expression of cyclin E in the HCT116 cells. Reversely, we observed a slight down-regulation of this protein in the other cell lines. A reference compound (3-AP) caused overexpression od cyclin E in all testes cell lines. Moreover, the western blot analysis revealed the influence of L^9, especially, by the significant decrease of the expression of p21 protein in HCT116 cells. On the other hand, after treatment with L^9, we observed the considerable down-regulation of p21 in the MCF-7 cells. We observed the similar pattern in changes in the expression of the cdc2 protein. Investigated compound influenced on the slight down-regulation of the cdc2 in the HCT116, and MCF-7 cell lines. In the case of 3-AP this effect was much stronger (MCF-7). This suggests that the TSCs have no influence on the entry of cells into the mitosis phase of the cell cycle. The obtained results indicate that the novel analogs of Triapine induced the arrest of the cell cycle in the G1/S phase and thus triggered apoptosis. Typically, this effect is connected with the activation of caspases–a family of endoproteases that participates in triggering the cellular response to damage. Caspase-8 is the initiator that participates in the extrinsic apoptosis pathway. Its activation comes via dimerization and leads to the initiation of the executioner caspases (-3, -6, -7) or activates the intrinsic pathway of apoptosis. The second type of cell death is

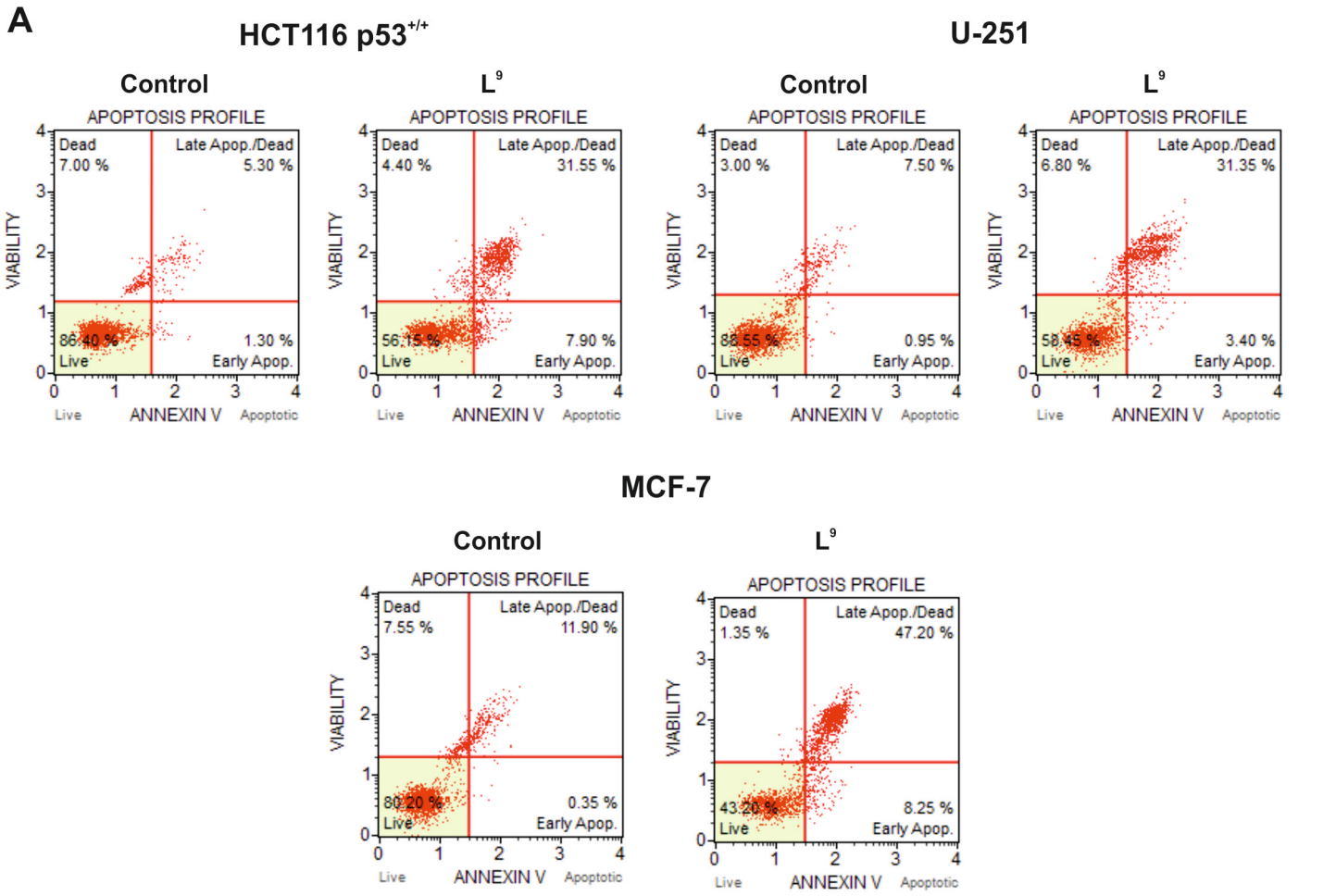

B

	HCT116 p53+/+		U-251		MCF-7	
	Control	L9	Control	L9	Control	L9
Live [%]	87.70± 1.84	59.79± 13.32	85.65± 4.10	62.03± 3.58	87.38± 10.15	41.20± 2.83
Total Apoptotic [%]	7.58± 1.38	31.64± 10.28	9.48± 1.45	31.20± 3.55	8.75± 4.95	55.15± 0.42

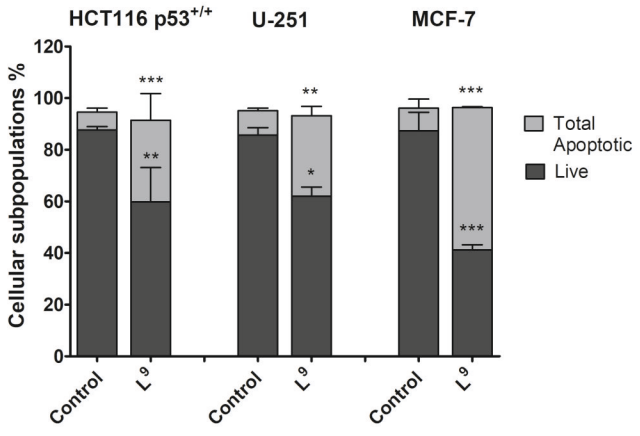

Fig 6. Evaluation of the induction of apoptosis in the HCT116 p53$^{+/+}$, U-251 and MCF-7 cells 48 h after treatment with L^9. The histograms show the percentage of early and late apoptosis for one of three independent experiments (**A**). The table shows the mean ± SD percentage of live, early and late apoptotic cells from three independent experiments (**B**). Data were analyzed using one-way ANOVA with Bonferroni's post-hoc test: *p<0.05, **p<0.01, ***p<0.001 compared to the control (**C**).

https://doi.org/10.1371/journal.pone.0188767.g006

also called mitochondrial apoptosis and is connected with the release of cytochrome c into the cytosol [78,79]. Therefore, we examined the effect of a 24 h treatment with L^9 on the regulation

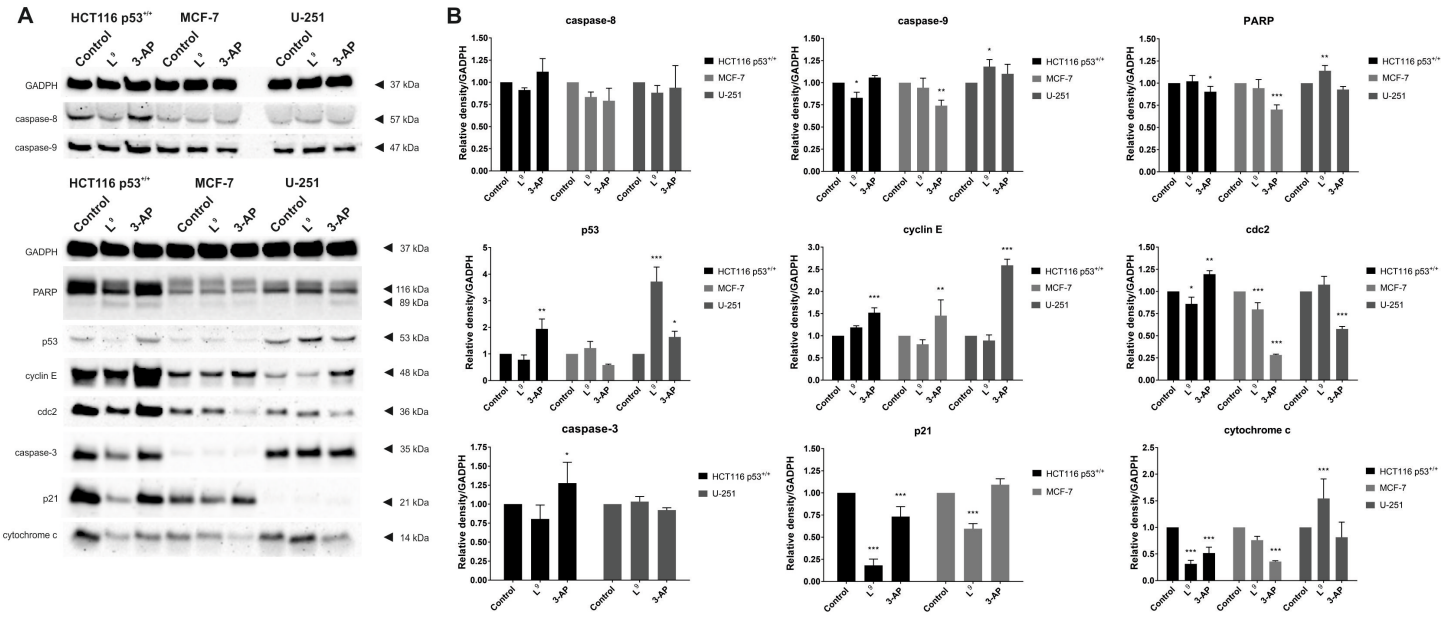

Fig 7. The effect of L^9 on the expression of the proteins: GADPH, PARP, caspase-3, 8, 9, p53, cyclin E, cdc2, p21, and cytochrome c, in the HCT116 $p53^{+/+}$, U-251 and MCF-7 cells. (A). Densitometric analyses of western blot images. Expression level signals are relative to GADPH expression. Data were analyzed using one-way ANOVA with Bonferroni's post-hoc test: *p<0.05, **p<0.01, ***p<0.001 compared to the control (**B**).

https://doi.org/10.1371/journal.pone.0188767.g007

of cytochrome c, and caspase-3, 8, 9 proteins. Additionally we explored another proteins, which are involved in the apoptosis pathway: p53, and PARP. Similar to previous results, we observed some differences among the investigated cell lines, which may be associated with various lengths of their cell cycle. The obtained results confirm that treatment with L^9 induces the release of cytochrome c from the mitochondria into the cytosol in case of HCT116 cells. Additionally, we observed a slight down-regulation of cytochrome c in and MCF-7. For 3-AP we detected release of cytochrome c in all tested cell lines. To further elucidate the mechanism, we evaluated the influence of L^9 on the extrinsic pathway of caspases activation.

In the case of caspase-3 we did not detect any significant changes in its expression for HCT116, and U-251 cell lines. It is commonly known that MCF-7 cell line do not express caspase-3 [80], and thus we investigate another caspase proteins. In general we observed the same pattern for caspase-8. In the case of caspase-9 we detected slight down-regulation for HCT116, and no influence on the MCF-7 cell line. A small up-regulation occurred for glioma cells. Results of caspases expression may indicate another pathway of the apoptosis triggering. Another investigated protein was p53, which is involved in many proliferating, and survival signals in cell. We detected interesting dependence in glioma cells, for which the upregulation of p53 was noticed. However it should be highlighted that U-251 cells are mutants with R273H missense mutation of p53. This resulted in normally expressed protein, that is able to cross the nucleus and interact with DNA [81,82]. Although overexpression of mutp53 in U-251 cells do not correlate with apoptosis. With this in mind increased level of cytochrome c and caspase-9 may suggest p53-independent apoptosis pathway. In colon and breast cancer influence of p53 protein was unnoticeable. Very popular protein for detection of cell death is PARP. Analysis of the lines on the gel indicated PARP cleavage for HCT116. This was also observed for glioma cell, but just for 3-AP. Summarizing, our hypothesis suggests influence of the cytochrome c (HCT116, MCF-7), and PARP (HCT116) on the apoptotic pathway.

Conclusions

In the current study, a new class of TSCs, piperazinylogs of Triapine, was designed to fulfill the di-substitution pattern at the TSCs N4 position, which is a crucial prerequisite for the high activity of the previously obtained TSC compounds–DpC and Dp44mT. We tested the important physicochemical characteristics of the novel compounds L^1-L^{12}. The studied ligands are neutral at physiological pH, which allows them to permeate cell membranes and bind cellular Fe pools more readily than less lipid-soluble ligands, e.g. DFO.

The selectivity and anti-cancer activity of the novel TSCs were examined in a variety of cancer cell types. In general, the novel compounds demonstrated the greatest promise as anti-cancer agents with both a potent and selective anti-proliferative activity (Table 2). Accordingly, structure-activity relationship studies revealed that the combination of the piperazine ring with Triapine allows potent and selective anticancer chelators that warrant further *in vivo* examination to be identified. In particular, compounds L^6 and L^{10} with a fluorine atom within the piperazine fragment appeared to enhance the activity and selectivity of the new analogs.

Significantly, this study proved the importance of the di-substitution pattern of the amine N4 function, thus identifying new potent and selective anticancer chelators that warrant further *in vivo* examination.

Experimental section

Chemistry

Microwave reactions were carried out in a Discover® BenchMate™ (CEM) microwave equipped with 10 mL vessels. Melting point measurements were determined in a Stanford Research Systems OptiMelt (MPA 100). ^{1}H and ^{13}C NMR spectra were recorded on a Bruker Ascend 500 MHz spectrometer at frequencies of 500 MHz and 126 MHz and a Bruker Avance III 400 MHz FT-NMR spectrometer at frequencies of 400 MHz and 101 MHz using DMSO-d_6 as the solvent and TMS as the internal standard. The NMR solvents were purchased from ACROS Organics. The chemical shifts (δ) are given in ppm and the coupling constants (J) values are reported in hertz (Hz). The spin multiplicities are described as s (singlet), d (doublet), dd (double of doublets), t (triplet), q (quartet) and m (multiplet). All evaporations were performed on a rotary evaporator under diminished pressure at 60˚C. All reagents and solvents were purchased from ACROS Organics, Asta-Tech, Maybridge, Santa Cruz Biotechnology and Sigma-Aldrich and were used without further purification.

The purity of all compounds were tested using the HPLC/MS method. The HPLC–MS analyses were performed on Varian model 920 liquid chromatograph equipped with the Varian 900-LC model autosampler, the gradient pump, the Varian Pro Star 510 model column oven, the Varian 380-LC model evaporative light scattering detection (ELSD) detector. This was coupled with Varian 500-MS IT. HRMS were determined with high resolution mass spectrometer Waters LCT Premier XE with electrospray ionisation (ESI).

General procedure for the synthesis of thiosemicarbazides. The mixtures of (1,1'-thiocarbonyl) bis-1H-imidazole (5 mmol) and a suitable derivative of piperazine (5 mmol) in methylene chloride (25 mL) were stirred for 24 h at room temperature. The solutions were extracted with distilled water three times and the organic phases were dried over anhydrous magnesium sulfate, filtered and then evaporated on a rotary evaporator. The obtained derivatives of thioketone were added to a solution of 5 mmol of hydrazine hydrate in 25 mL of ethanol at room temperature. The reaction mixture was refluxed for 2 h and cooled to obtain a precipitate, which was collected via filtration. The final thiosemicarbazides were crystallized from methanol.

4-phenylpiperazine-1-carbothiohydrazide (**K[1]**)

White powder; yield 69%; mp: 173–174; ^{1}H-NMR (400 MHz, d_6-DMSO, ppm): δ 3.15 (s, 4H, CH_2), 3.87 (s, 4H, CH_2), 6.80 (t, 1H; J = 7.1 Hz), 6.95 (d, 2H; J = 8.0 Hz), 7.22 (t, 2H; J = 7.7 Hz), 9.17 (s, 1H, NH). ^{13}C-NMR (126 MHz, d_6-DMSO, ppm): δ 48.3; 56.5; 116.0; 119.7; 129.4; 151.1; 183.0. MS (ESI$^+$): *m/z* calculated for $C_{11}H_{16}N_4S$: 236.11, found: 237.64 $[M+H]^+$, 276.05 $[M+K]^+$.

4-(4-fluorophenyl)piperazine-1-carbothiohydrazide (**K[2]**)

Light pink powder; yield 97%; mp: 180–181; ^{1}H-NMR (400 MHz, d_6-DMSO, ppm): δ 3.09 (m, 4H, CH_2), 3.87 (m, 4H, CH_2), 4.77 (s, 2H, NH_2), 6.97 (m, 2H, CH), 7.05 (m, 2H, CH), 9.19 (s, 1H, NH). ^{13}C-NMR (101 MHz, d_6-DMSO, ppm): δ 40.3; 49.1; 115.9; 117.9; 148.0; 157.8; 183.0. MS (ESI$^+$): *m/z* calculated for $C_{11}H_{15}FN_4S$: 254.10, found: 276.30 $[M+Na]^+$.

4-(4-chlorophenyl)piperazine-1-carbothiohydrazide (**K[3]**)

White powder; yield 90%; mp: 195–196; ^{1}H-NMR (500 MHz, d_6-DMSO, ppm): δ 3.16 (t, 4H, J = 5.2 Hz), 3.86 (t, 4H, J = 5.2 Hz), 6.95 (m, 2H, CH), 7.24 (m, 2H, CH), 9.18 (s, 1H, NH). ^{13}C-NMR (126 MHz, d_6-DMSO, ppm): δ 47.3; 48.0; 117.3; 123.0; 129.1; 149.8; 182.9. MS (ESI$^+$): *m/z* calculated for $C_{11}H_{15}ClN_4S$: 270.07, found: 270.35 $[M]^+$.

4-(4-methoxyphenyl)piperazine-1-carbothiohydrazide (**K[4]**)

White powder; yield 81%; mp: 194–195; ^{1}H-NMR (400 MHz, d_6-DMSO, ppm): δ 3.00 (m, 4H, CH_2), 3.68 (s, 3H, CH_3), 3.86 (m, 4H, CH_2), 4.76 (s, 2H, NH_2), 6.83 (m, 2H, CH), 6.92 (m, 2H, CH), 9.17 (s, 1H, NH).^{13}C-NMR (101 MHz, d_6-DMSO, ppm): δ 19.0; 49.9; 56.5; 114.8; 118.2; 145.4; 153.7; 183.1. MS (ESI$^+$): *m/z* calculated for $C_{12}H_{18}N_4OS$: 266.12, found: 288.02 $[M+Na]^+$.

4-(4-cyanophenyl)piperazine-1-carbothiohydrazide (**K[5]**)

White powder; yield 86%; mp: 179–180; ^{1}H-NMR (400 MHz, d_6-DMSO, ppm): δ 3.42 (m, 4H, CH_2), 3.88 (m, 4H, CH_2), 4.76 (s, 2H, NH_2), 6.99 (m, 2H, CH), 7.59 (m, 2H, CH), 9.15 (s, 1H, NH). ^{13}C-NMR (126 MHz, d_6-DMSO, ppm): δ 40.6; 48.8; 98.6; 114.3; 120.5; 133.8; 153.1; 182.9. MS (ESI$^+$): *m/z* calculated for $C_{12}H_{15}N_5S$: 261.10, found: 284.75 $[M+Na]^+$.

4-[2-nitro-4-(trifluoromethyl)phenyl]piperazine-1-carbothiohydrazide (**K[6]**)

Light orange crystals; yield 75%; mp: 167–168; ^{1}H-NMR (500 MHz, d_6-DMSO, ppm): δ 3.26 (m, 4H, CH_2), 3.88 (m, 4H, CH_2), 4.76 (s, 2H, NH_2), 7.44 (d, 1H; J = 8.8 Hz), 7.86 (dd, 1H; J_1 = 9.0 Hz, J_2 = 2.3 Hz), 8.17 (dd, 1H; J_1 = 2.3 Hz, J_2 = 0.9 Hz), 9.15 (s, 1H, NH). ^{13}C-NMR (126 MHz, d_6-DMSO, ppm): δ 46.9; 49.4; 119.7; 121.2; 123.0; 124.4; 130.5; 139.1; 147.5; 183.0. MS (ESI$^+$): *m/z* calculated for $C_{12}H_{14}F_3N_5O_2S$: 349.08, found: 349.05 $[M]^+$.

tert-butyl 4-(hydrazinylcarbonothioyl)piperazine-1-carboxylate (**K[7]**)

White powder; yield 70%; mp: 165–167; ^{1}H-NMR (500 MHz, d_6-DMSO, ppm): δ 1.41 (s, 9H, CH_3), 3.32 (m, 4H, CH_2), 3.71 (m, 4H, CH_2), 4.72 (s, 2H, NH_2), 9.11 (s, 1H, NH). ^{13}C-NMR (126 MHz, d_6-DMSO, ppm): δ 19.0; 28.5; 47.4; 49.0; 79.6; 154.3; 183.1. MS (ESI$^+$): *m/z* calculated for $C_{10}H_{20}N_4O_2S$: 260.13, found: 283.77 $[M+Na]^+$.

4-(pyridin-2-yl)piperazine-1-carbothiohydrazide (**K[8]**)

White powder; yield 98%; mp: 172–173; ^{1}H-NMR (400 MHz, d_6-DMSO, ppm): δ 3.18 (s, 4H, CH_2), 3.85 (m, 4H, CH_2), 4.77 (s, 2H, NH_2), 6.83 (m, 1H, CH), 7.56 (m, 1H, CH), 8.13 (m, 1H, CH), 9.13 (s, 1H, NH). ^{13}C-NMR (101 MHz, d_6-DMSO, ppm): δ 39.6; 51.0; 107.6; 113.7; 138.0; 148.0; 159.1; 183.0. MS (ESI$^+$): *m/z* calculated for $C_{10}H_{15}N_5S$: 237.10, found: 237.65 $[M]^+$.

4-[5-(trifluoromethyl)pyridin-2-yl]piperazine-1-carbothiohydrazide (**K[9]**)

White powder; yield 70%; mp: 206–207; ^{1}H-NMR (400 MHz, d_6-DMSO, ppm): δ 3.70 (s, 4H, CH_2), 3.87 (s, 4H, CH_2), 4.76 (s, 2H, NH_2), 6.93 (d, 1H, J = 9.1 Hz), 7.82 (s, 1H, CH), 8.42 (s, 1H, CH), 9.14 (s, 1H, NH). ^{13}C-NMR (101 MHz, d_6-DMSO, ppm): δ 43.8; 46.9; 49.1; 106.7;

134.9; 145.6; 145.7; 160.3; 183.0. MS (ESI^+): *m/z* calculated for $C_{11}H_{14}F_3N_5S$: 305.09, found: 305.25 $[M]^+$.

4-[3-chloro-5-(trifluoromethyl)pyridin-2-yl]piperazine-1-carbothiohydrazide (**K[10]**)

White powder; yield 85%; mp: 191–192; ^{1}H-NMR (500 MHz, d_6-DMSO, ppm): δ 3.51 (m, 4H, CH_2), 3.88 (m, 4H, CH_2), 4.83 (s, 2H, NH_2), 8.20 (d, 1H; *J* = 2.1 Hz), 8.56 (s, 1H, CH), 9.18 (s, 1H, NH). ^{13}C-NMR (126 MHz, d_6-DMSO, ppm): δ 47.3; 48.1; 120.2; 122.8; 125.0; 136.8; 143.5; 159.7; 183.2. MS (ESI^+): *m/z* calculated for $C_{11}H_{13}ClF_3N_5S$: 339.05, found: 340.28 $[M+H]^+$.

4-(pyrimidin-2-yl)piperazine-1-carbothiohydrazide (**K[11]**)

White powder; yield 92%; mp: 208–209; ^{1}H-NMR (500 MHz, d_6-DMSO, ppm): δ 3.75 (m, 4H, CH_2), 3.83 (m, 4H, CH_2), 4.76 (s, 2H, NH_2), 6.66 (t, 1H, *J* = 4.7 Hz), 8.38 (d, 2H, *J* = 4.7 Hz), 9.13 (s, 1H, NH). ^{13}C-NMR (126 MHz, d_6-DMSO, ppm): δ 43.2; 47.3; 110.9; 158.4; 161.5; 183.0. MS (ESI^+): *m/z* calculated for $C_9H_{14}N_6S$: 238.10, found: 238.35 $[M]^+$.

4-(pyrazin-2-yl)piperazine-1-carbothiohydrazide (**K[12]**)

Light pink crystals; yield 88%; mp: 177–178; ^{1}H-NMR (500 MHz, d_6-DMSO, ppm): δ 3.61 (m, 4H, CH_2), 3.87 (m, 4H, CH_2), 4.77 (s, 2H, NH_2), 7.86 (d, 1H; *J* = 2.7 Hz), 8.09 (dd, 1H; J_1 = 2.7 Hz, J_2 = 1.5 Hz), 8.31 (d, 1H, *J* = 1.5 Hz), 9.16 (s, 1H, NH). ^{13}C-NMR (126 MHz, d_6-DMSO, ppm): δ 43.7; 47.0; 131.7; 133.0; 141.9; 154.7; 182.9. MS (ESI^+): *m/z* calculated for $C_9H_{14}N_6S$: 238.10, found: 238.57 $[M+H]^+$.

General procedure for synthesis of thiosemicarbazones. We added two drops of glacial acetic acid as a catalyst to the mixtures of thiosemicarbazides (0.5 mmol) and 3-aminopyridine-2-carboxaldehyde (0.5 mmol) in ethanol (5 mL). The glass tubes were sealed and placed into a microwave reactor at 83 °C for 20 minutes (the reactor power did not exceed 50 W). The obtained thiosemicarbazones were crystallized from methanol.

N'-[(3-aminopyridin-2-yl)methylidene]-4-phenylpiperazine-1-carbothiohydrazide (**L[1]**)

Light yellow crystals; yield 83%; mp: 189–190; ^{1}H-NMR (400 MHz, d_6-DMSO, ppm): δ 3.26 (s, 4H, CH_2), 4.09 (s, 4H, CH_2), 6.82 (t, 1H; *J* = 7.3 Hz), 6.99 (d, 2H; *J* = 8.2 Hz), 7.10 (m, 2H, CH), 7.18 (s, 2H, NH_2), 7.25 (t, 2H; *J* = 7.8 Hz), 7.84 (dd, 1H; J_1 = 4.0 Hz, J_2 = 1.6 Hz), 8.53 (s, 1H, CH), 11.44 (s, 1H, NH). ^{13}C-NMR (126 MHz, d_6-DMSO, ppm): δ 48.3; 48.6; 116.0; 119.6; 122.4; 124.5; 129.5; 134.2; 137.2; 144.2; 149.5; 150.9; 180.0. HRMS (ESI): *m/z* calculated for $C_{17}H_{21}N_6S$: 341.1548, found: 341.1547 $[M+H]^+$.

N'-[(3-aminopyridin-2-yl)methylidene]-4-(4-fluorophenyl)piperazine-1-carbothiohydrazide (**L[2]**)

Yellow crystals; yield 70%; mp: 210–211; ^{1}H-NMR (400 MHz, d_6-DMSO, ppm): δ 3.18 (s, 4H, CH_2), 4.08 (s, 4H, CH_2), 6.96–7.03 (m, 2H, CH), 7.04–7.13 (m, 4H, CH), 7.17 (s, 2H, NH_2), 7.84 (d, 1H; *J* = 3.9 Hz), 8.53 (s, 1H, CH), 11.44 (s, 1H, NH). ^{13}C-NMR (126 MHz, d_6-DMSO, ppm): δ 48.6; 49.3; 115.8; 117.9; 122.4; 124.5; 134.2; 137.2; 144.2; 147.8; 149.5; 155.8; 157.6; 180.1. HRMS (ESI): *m/z* calculated for $C_{17}H_{20}FN_6S$: 359.1454, found: 359.1466 $[M+H]^+$.

N'-[(3-aminopyridin-2-yl)methylidene]-4-(4-chlorophenyl)piperazine-1-carbothiohydrazide (**L[3]**)

Yellow powder; yield 83%; mp: 206–207; ^{1}H-NMR (500 MHz, d_6-DMSO, ppm): δ 3.27 (t, 4H, *J* = 5.2 Hz), 4.08 (t, 4H, *J* = 5.3 Hz), 6.99 (m, 2H, CH), 7.06–7.08 (dd, 1H; J_1 = 8.3 Hz, J_2 = 4.2 Hz), 7.09–7.12 (dd, 1H; J_1 = 8.4 Hz, J_2 = 1.6 Hz), 7.14–7.22 (s, 2H, NH_2), 7.25–7.28 (m, 2H, CH), 7.84 (dd, 1H; J_1 = 4.2 Hz, J_2 = 1.6 Hz), 8.53 (s, 1H, CH), 11.45 (s, 1H, NH). ^{13}C-NMR (126 MHz, d_6-DMSO, ppm): δ 48.0; 48.4; 117.3; 122.5; 123.1; 124.5; 129.1; 134.2; 137.2; 144.2; 149.5; 149.7; 180.1. HRMS (ESI): *m/z* calculated for $C_{17}H_{20}ClN_6S$: 375.1159, found: 375.1155 $[M+H]^+$.

N'-[(3-aminopyridin-2-yl)methylidene]-4-(4-methoxyphenyl)piperazine-1-carbothiohydrazide (**L[4]**)

Yellow powder; yield 59%; mp: 195–196; ^{1}H-NMR (400 MHz, d_6-DMSO, ppm): δ 3.11 (s, 4H, CH_2), 3.70 (s, 3H, CH_3), 4.07 (s, 4H, CH_2), 6.85 (m, 2H, CH), 6.96 (m, 2H, CH), 7.09 (m, 2H, CH), 7.17 (s, 2H, NH_2), 7.84 (dd, 1H; J_1 = 4.1 Hz, J_2 = 1.7 Hz), 8.52 (s, 1H, CH), 11.43 (s, 1H, NH). ^{13}C-NMR (101 MHz, d_6-DMSO, ppm): δ 48.8; 50.0; 55.7; 114.8; 118.3; 122.4; 124.5; 134.2; 137.1; 144.2; 145.3; 149.4; 153.7; 180.1. HRMS (ESI): *m/z* calculated for $C_{18}H_{23}N_6OS$: 371.1654, found: 371.1645 $[M+H]^+$.

N'-[(3-aminopyridin-2-yl)methylidene]-4-(4-cyanophenyl)piperazine-1-carbothiohydrazide (**L^5**)

Light orange powder; yield 74%; mp: 209–210; ^{1}H-NMR (400 MHz, d_6-DMSO, ppm): δ 3.53 (s, 4H, CH_2), 4.10 (s, 4H, CH_2), 7.02 (d, 2H; *J* = 8.8 Hz), 7.09 (m, 2H, CH), 7.17 (s, 2H, NH_2), 7.62 (d, 2H; *J* = 8.7 Hz), 7.84 (dd, 1H; J_1 = 4.1 Hz, J_2 = 1.6 Hz), 8.54 (s, 1H, CH), 11.42 (s, 1H, NH). ^{13}C-NMR (126 MHz, d_6-DMSO, ppm): δ 45.8; 47.9; 98.5; 114.0; 120.6; 122.5; 124.5; 133.8; 134.2; 137.2; 144.2; 149.6; 152.9; 179.9. HRMS (ESI): *m/z* calculated for $C_{18}H_{20}N_7S$: 366.1501, found: 366.1503 $[M+H]^+$.

N'-[(3-aminopyridin-2-yl)methylidene]-4-[2-nitro-4-(trifluoromethyl)phenyl]piperazine-1-carbothiohydrazide (**L^6**)

Yellow powder; yield 75%; mp: 179–180; ^{1}H-NMR (500 MHz, d_6-DMSO, ppm): δ 3.38 (m, 4H, CH_2), 4.09 (m, 4H, CH_2), 7.07 (dd, 1H; J_1 = 8.3 Hz, J_2 = 4.2 Hz), 7.11 (dd, 1H; J_1 = 8.4 Hz, J_2 = 1.6 Hz), 7.13–7.21 (s, 2H, NH_2), 7.47 (d, 1H; *J* = 8.9 Hz), 7.83–7.91 (m, 2H, CH), 8.20 (d, 1H, *J* = 2.7 Hz), 8.53 (s, 1H, CH), 11.42 (s, 1H, NH). ^{13}C-NMR (126 MHz, d_6-DMSO, ppm): δ 19.0; 47.9; 49.3; 56.5; 121.1; 122.5; 123.0; 124.4; 130.5; 134.2; 137.2; 138.9; 144.3; 147.5; 149.7; 180.1. HRMS (ESI): *m/z* calculated for $C_{18}H_{19}F_3N_7O_2S$: 454.1293, found: 474.1269 $[M+H]^+$.

tert-butyl 4-({2-[(3-aminopyridin-2-yl)methylidene]hydrazinyl}carbonothioyl)piperazine-1-carboxylate (**L^7**)

Yellow powder; yield 20%; mp: 193–194; ^{1}H-NMR (500 MHz, d_6-DMSO, ppm): δ 1.43 (s, 9H, CH_3), 3.44 (m, 4H, CH_2), 3.93 (m, 4H, CH_2), 7.05–7.12 (m, 2H, CH), 7.13–7.19 (s, 2H, NH_2), 7.84 (dd, 1H; J_1 = 4.2 Hz, J_2 = 1.6 Hz), 8.51 (s, 1H, CH), 11.39 (s, 1H, NH). ^{13}C-NMR (126 MHz, d_6-DMSO, ppm): δ 28.5; 48.4; 79.7; 122.8; 124.5; 133.9; 136.9; 144.3; 149.2; 154.3; 180.2. HRMS (ESI): *m/z* calculated for $C_{16}H_{25}N_6O_2S$: 365.1760, found: 365.1769 $[M+H]^+$.

N'-[(3-aminopyridin-2-yl)methylidene]-4-(pyridin-2-yl)piperazine-1-carbothiohydrazide (**L^8**)

Yellow crystals; yield 38%; mp: 210–211; ^{1}H-NMR (400 MHz, d_6-DMSO, ppm): δ 3.64 (m, 4H, CH_2), 4.07 (m, 4H, CH_2), 6.68 (m, 1H, CH), 6.86 (d, 1H; *J* = 8.6 Hz), 7.09 (m, 2H, CH), 7.18 (s, 2H, NH_2), 7.58 (m, 1H, CH), 7.84 (dd, 1H; J_1 = 4.1 Hz, J_2 = 1.6 Hz), 8.15 (d, 1H, *J* = 4.9 Hz), 8.54 (s, 1H, CH), 11.41 (s, 1H, NH). ^{13}C-NMR (101 MHz, d_6-DMSO, ppm): δ 44.4; 48.3; 107.5; 113.7; 122.5; 124.5; 134.2; 137.1; 138.1; 144.2; 148.0; 149.5; 159.0; 180.1. HRMS (ESI): *m/z* calculated for $C_{16}H_{20}N_7S$: 342.1501, found: 342.1514 $[M+H]^+$.

N'-[(3-aminopyridin-2-yl)methylidene]-4-[5-(trifluoromethyl)pyridin-2-yl]piperazine-1-carbothiohydrazide (**L^9**)

Yellow crystals; yield 47%; mp: 232–233; ^{1}H-NMR (400 MHz, d_6-DMSO, ppm): δ 3.80 (s, 4H, CH_2), 4.09 (s, 4H, CH_2), 6.97 (d, 1H; *J* = 9.1 Hz), 7.08 (m, 2H, CH), 7.18 (s, 2H, NH_2), 7.85 (m, 2H, CH), 8.46 (d, 1H, *J* = 2.5 Hz), 8.54 (s, 1H, CH), 11.42 (s, 1H, NH). ^{13}C-NMR (101 MHz, d_6-DMSO, ppm): δ 43.8; 47.9; 106.7; 113.8; 122.5; 124.5; 126.4; 134.2; 135.0; 137.1; 144.2; 145.7; 149.6; 160.3; 180.0. HRMS (ESI): *m/z* calculated for $C_{17}H_{19}F_3N_7S$: 410.1374, found: 410.1365 $[M+H]^+$.

4.1.2.10. N'-[(3-aminopyridin-2-yl)methylidene]-4-[3-chloro-5-(trifluoromethyl)pyridin-2-yl]piperazine-1-carbothiohydrazide (**L^{10}**)

Dark yellow powder; yield 64%; mp: 199–200; ^{1}H-NMR (500 MHz, d_6-DMSO, ppm): δ 3.63 (m, 4H, CH_2), 4.10 (m, 4H, CH_2), 7.05–7.09 (dd, 1H; J_1 = 8.3 Hz, J_2 = 4.2 Hz), 7.09–7.12 (dd, 1H; J_1 = 8.3 Hz, J_2 = 1.6 Hz), 7.14–7.21 (s, 2H, NH_2), 7.84 (dd, 1H; J_1 = 4.1 Hz, J_2 = 1.6 Hz),

8.23 (d, 1H, J = 2.2 Hz), 8.53 (s, 1H, CH), 8.59 (dd, 1H; J_1 = 2.3 Hz, J_2 = 1.1 Hz), 11.44 (s, 1H, NH). ^{13}C-NMR (126 MHz, d_6-DMSO, ppm): δ 48.1; 48.3; 119.1; 120.0; 122.5; 124.5; 125.0; 134.2; 136.9; 137.2; 143.6; 144.2; 149.6; 159.5; 180.3. HRMS (ESI): *m/z* calculated for $C_{17}H_{18}ClF_3N_7S$: 444.0985, found: 464.0988 $[M+H]^+$.

N'-[(3-aminopyridin-2-yl)methylidene]-4-(pyrimidin-2-yl)piperazine-1-carbothiohydrazide (**L^{11}**)

Light yellow powder; yield 39%; mp: 198–199; ^{1}H-NMR (500 MHz, d_6-DMSO, ppm): δ 3.86 (m, 4H, CH_2), 4.05 (m, 4H, CH_2), 6.69 (t, 1H, J = 4.7 Hz), 7.07 (dd, 1H; J_1 = 8.3 Hz, J_2 = 4.2 Hz), 7.11 (dd, 1H; J_1 = 8.3 Hz, J_2 = 1.6 Hz), 7.13–7.22 (s, 2H, NH_2), 7.84 (dd, 1H; J_1 = 4.2 Hz, J_2 = 1.6 Hz), 8.41 (d, 2H, J = 4.7 Hz), 8.53 (s, 1H, CH), 11.43 (s, 1H, NH). ^{13}C-NMR (126 MHz, d_6-DMSO, ppm): δ 43.2; 48.4; 111.0; 122.5; 124.5; 134.2; 137.1; 144.2; 149.4; 158.5; 161.5; 180.1. HRMS (ESI): *m/z* calculated for $C_{15}H_{19}N_8S$: 343.1453, found: 343.1464 $[M+H]^+$.

N'-[(3-aminopyridin-2-yl)methylidene]-4-(pyrazin-2-yl)piperazine-1-carbothiohydrazide (**L^{12}**)

Yellow crystals; yield 70%; mp: 217–218; ^{1}H-NMR (500 MHz, d_6-DMSO, ppm): δ 3.72 (m, 4H, CH_2), 4.09 (m, 4H, CH_2), 7.05–7.12 (m, 2H, CH), 7.14–7.22 (s, 2H, NH_2), 7.84 (dd, 1H; J_1 = 4.2 Hz, J_2 = 1.6 Hz), 7.88 (d, 1H; J = 2.6 Hz), 8.12 (dd, 1H; J_1 = 2.7 Hz, J_2 = 1.5 Hz), 8.35 (d, 1H, J = 1.6 Hz), 8.54 (s, 1H, CH), 11.44 (s, 1H, NH). ^{13}C-NMR (126 MHz, d_6-DMSO, ppm): δ 43.8; 48.0; 122.5; 124.5; 131.7; 133.1; 134.2; 137.2; 141.9; 144.2; 149.6; 154.7; 180.0. HRMS (ESI): *m/z* calculated for $C_{15}H_{19}N_8S$: 343.1453, found: 343.1454 $[M+H]^+$.

Materials and physico-chemical measurements

Starting Materials and Solvents. The solution studies were carried out in bidistilled water. All the chemicals were commercial products of reagent grade and were used without further purification.

The Iron(III) stock solution was prepared from $FeCl_3{\cdot}6H_2O$ (Aldrich) in 1.01×10^{-2} M HCl (Chempur 38%) immediately before use. The Copper(II) solution was prepared from $CuCl_2 \cdot 2H_2O$ (Aldrich). All metal stock solutions were standardized using ICP-AES. The HCl solution was titrated using standardized NaOH (0.1 M Fluka standard solution).

pH-dependent UV-visible titrations. To determine the acid-base properties of the studied ligands, UV-visible spectrophotometric experiments as a function of p[H] were carried out in the pH range 2–11.

The isosbestic curves were used to determine the ability of a binding event of the ligand with Fe(III) and Cu(II). A series of six samples were prepared for each ligand. The ligand was dissolved in 0.1 M KCl in MeOH/H_2O (80/20 w/w) ionic strength and mixed with a freshly prepared $FeCl_3{\cdot}6H_2O$ or $CuCl_2{\cdot}2H_2O$ solution at various ratio concentrations of the metal ions. The complex that was formed for each reaction mixture was allowed to stand for 30 min before the analysis. Absorption spectra were recorded in a Hellma quartz optical cell (1 cm) on a Jasco V630 spectrophotometer.

All the titrations were carried out on 3.2 mL samples. The metal-ligand system titrations were performed on solutions of ligand concentrations of $5x10^{-5}$ M and metal-to-ligand molar ratios of 1:1, 1:2, 1:3, 1:4 and 1:5.

UV-Visible titrations were also carried out. The absorption spectra (200–800 nm) were recorded using a Jasco V630 spectrophotometer. The initial pH of 3.2 mL ligand samples was adjusted to be acidic or basic and the titration of the solution was then carried out by adding known volumes of NaOH or HCl, respectively. The spectrophotometric data were fitted using the HypSpec [83] program. Distribution diagrams of the species were calculated using Hyperquad Simulation and Speciation (HySS) software [84].

Antitumor activity

Cell lines. The human colon carcinoma cell line HCT116 wild type ($p53^{+/+}$), human breast carcinoma cell line MCF-7 and glioblastoma cell line Hs683 were obtained from ATCC. The glioma cell line U-251 was purchased from Sigma Aldrich and the normal human fibroblast cell lines NHDF from PromoCell. The human colon cancer cell line HCT116 with a p53 deletion ($p53^{-/-}$) was kindly provided by Prof. M. Rusin from the Maria Sklodowska-Curie Memorial Cancer Centre and Institute of Oncology in Gliwice, Poland. Cells were grown as monolayer cultures in Dulbecco's modified Eagle's medium with an antibiotic gentamicin (200 μL/100 mL medium) in 75 cm^2 flasks (Nunc). DMEM for HCT116, MCF-7, U-251, Hs683 were supplemented with 12% heat-inactivated fetal bovine serum (Sigma) and for NHDF with 15% non-inactivated fetal bovine serum (Sigma). All the cell lines were cultured under standard conditions at 37˚C in a humidified atmosphere at 5% CO_2.

Cytotoxicity studies. The cells were seeded in 96-well plates (Nunc) at a density of 5,000 cells/well (HCT116, MCF-7, U-251, Hs683) and 4,000 cells/well (NHDF) and incubated at 37˚C for 24 h. The assay was performed following a 72 h incubation with varying concentrations of the compounds that were tested. Then, 20 μL of The CellTiter 96®AQueous One Solution-MTS (Promega) solution was added to each well (with 100 μL DMEM without phenol red) and incubated for 1 h at 37˚C. The optical densities of the samples were analyzed at 490 nm using a multi-plate reader (Synergy 4, Bio Tek). Results were expressed as a percentage of the control and calculated as the inhibitory concentration (IC_{50}) values using GraphPad Prism 5. The IC_{50} parameter was defined as the compound concentration that was necessary to reduce the proliferation of cells to 50% of the untreated control. Each individual compound was tested in triplicate in a single experiment with each experiment being repeated four to five times.

Immunoblotting. The HCT116 ($p53^{+/+}$), U-251 and MCF-7 cells were seeded in 3 cm Petri dishes (Nunc) at a density of $0.5 \cdot 10^6$ cells/well and incubated overnight. The next day, a solution of L^9 at a four-fold IC_{50} concentration for each cell line was added and incubated for 24 h. Cells were harvested by trypsinization, washed with cold PBS and cell pellets were obtained by centrifugation at 2,000 rpm. Total cell lysates were obtained by dissolving the cell pellets in 150 μL of a RIPA buffer (Thermo Scientific) containing a Halt Protease Inhibitor Cocktail (Thermo Scientific) or Halt Phosphatase Inhibitor Cocktail (Thermo Scientific) along with 0.5 M EDTA and lysed for 20 min on ice on a rocking plate. The lysates were then sonicated, centrifuged at 10,000 rpm for 10 min at 4˚C and the supernatants were collected for further analysis. The protein concentration was determined using a Micro BCA™ Protein Assay Kit (Thermo Scientific) according to the manufacturer's instructions. Equal amounts of proteins (15 μg) were electrophoresed on SDS-Page gels and transferred onto a nitrocellulose membranes. The membranes were blocked in 5% non-fat milk prepared in PBS containing 0.1% Tween-20 (TPBS) for 1 h. After blocking, the membranes were incubated with specific primary antibodies: PARP, p53, $p21^{Waf1/Cip1}$, cdc2, cyclin E, cytochrome c, caspase-3,8,9 and GAPPH overnight at 4˚C, then washed and incubated with horseradish peroxidase (HRP)-conjugated secondary antibodies for 1 h at room temperature. All the antibodies were purchased from Cell Signaling and were diluted 1:1000 in 5% milk in TPBS. Finally, the membranes were washed and incubated with a SuperSignal™ West Pico Chemiluminescent Substrate (Thermo Scientific). The chemiluminescence signals were captured using a Chemi-Doc™ XRS+ System (BioRad). The experiments were performed at least three times.

Cell cycle assay. The HCT116 ($p53^{+/+}$), U-251 and MCF-7 cells were seeded in 3 cm Petri dishes (Nunc) at a density of $0.25 \cdot 10^6$ cells/well and incubated at 37˚C for 24 h. Then, the medium was removed and a freshly prepared solution of the tested compound–L^9 at a 0.5 μM

concentration was added. After 48 h of treatment, assays were performed using a Muse Cell-Cycle Kit (Millipore) according to the manufacturer's instructions. Briefly, the cells were collected, washed with cold PBS and were centrifuged at 300 g. Then, the cells were fixed in ice cold 70% ethanol and stored at -20˚C overnight. Afterwards, the cells were centrifuged and resuspended in 200 μL of Muse™ Cell Cycle Reagent and incubated for 30 min at room temperature in the dark. After staining, the cells were processed for cell cycle analysis using a Muse Cell Analyzer (Millipore). The experiments were performed at least three times.

Annexin V binding assay. The HCT116 ($p53^{+/+}$), U-251 and MCF-7 cells were seeded in 3 cm Petri dishes (Nunc) at a density of $0.25 \cdot 10^6$ cells/dish and incubated at 37˚C for 24 h. After treatment with 0.5 μM of L^9 for 48 h, the assays were performed using an Annexin V & Dead Cell Kit (Millipore) according to the manufacturer's instructions. Briefly, detached and adherent cells were collected and centrifuged at 500 g for 5 min. Next, the resuspended cells were incubated with 100 μL of Muse™ Annexin V & Dead Cell Reagent for 20 min at room temperature in the dark. After staining, the events for live, early and late apoptotic cells were counted using a Muse Cell Analyzer (Millipore). The experiments were performed at least three times.

Statistical analysis. All of data were expressed as the mean ± standard deviation (SD) of the results obtained from at least three independent experiments. Statistical differences was performed using one-way ANOVA with a Bonferroni post-hoc test (comparison to control). A p-value of 0.05 or less was considered to be statistically significant. GraphPad Prism v.5.0 software (GraphPad Software, USA) was used for analysis.

Supporting information

S1 Fig. The spectra and distribution forms of the ligands. (a) Absorption spectrophotometric titration vs. pH of the free L^1, L^8, L^{11} and L^{12} ligands; (b) electronic spectra of the protonated species; (c) concentration distribution curves for chosen ligands species. I = 0.1 M (KCl) in 80% (w/w) $MeOH/H_2O$; T = 25.0˚C; [L] = $5x10^{-5}$ M; pH 1.90–11.5.
(DOCX)

S2 Fig. The effect of L9 on the expression of the proteins–full view from Western blot analysis. (A) GADPH, (B) caspase-8, (C) caspase-9, (D) GADPH, (E) p53, (F) PARP, (G) cyclin E, (H) cdc2, (I) caspase-3, (J) p21, (K) cytochrome c.
(DOCX)

S1 Table. Changes in absorption spectra and isosbestic points for chosen ligands.
(DOCX)

S2 Table. Therapeutic indexes of the novel Triapine analogs describing their selectivity against normal cells. TI values I > 25, TI 2.5–25, TI < 2.5 were marked with red, yellow and grey color, respectively.
(DOCX)

Acknowledgments

The financial support of the National Center of Science grants 2014/13/D/NZ7/00322 (AMW), 2013/09/B/NZ7/00423 (RM) and NCBiR Warsaw ORGANOMET No: PBS2/A5/40/2014 (JP) is greatly appreciated.

Author Contributions

Conceptualization: Robert Musiol, Jaroslaw Polanski.

Formal analysis: Kamila Gajcy, Robert Musiol, Jaroslaw Polanski.

Investigation: Marta Rejmund, Anna Mrozek-Wilczkiewicz, Katarzyna Malarz, Monika Pyrkosz-Bulska, Mieczyslaw Sajewicz.

Methodology: Anna Mrozek-Wilczkiewicz.

Supervision: Jaroslaw Polanski.

Writing – original draft: Kamila Gajcy, Robert Musiol, Jaroslaw Polanski.

Writing – review & editing: Kamila Gajcy, Robert Musiol, Jaroslaw Polanski.

References

1. West DX, Padhye SB, Sonawane PB. Structural and physical correlations in the biological properties of transition metal heterocyclic thiosemicarbazone and S-alkyldithiocarbazate complexes. Complex Chemistry. 1991. pp. 1–50.
2. Brockman RW, Thomson JR, Bell MJ, Skipper HE. Observations on the antileukemic activity of pyridine-2-carboxaldehyde thiosemicarbazone and thiocarbohydrazone. Cancer Res. 1956; 16: 167–70. PMID: 13293659
3. Ma B, Goh BC, Tan EH, Lam KC, Soo R, Leong SS, et al. A multicenter phase II trial of 3-aminopyridine-2-carboxaldehyde thiosemicarbazone (3-AP, Triapine) and gemcitabine in advanced non-small-cell lung cancer with pharmacokinetic evaluation using peripheral blood mononuclear cells. Invest New Drugs. 2008; 26: 169–73. https://doi.org/10.1007/s10637-007-9085-0 PMID: 17851637
4. Fischer B, Kryeziu K, Kallus S, Heffeter P, Berger W, Kowol CR, et al. Nanoformulations of anticancer thiosemicarbazones to reduce methemoglobin formation and improve anticancer activity. RSC Adv. 2016; 6: 55848–55859.
5. Feun L, Modiano M, Lee K, Mao J, Marini A, Savaraj N, et al. Phase I and pharmacokinetic study of 3-aminopyridine-2-carboxaldehyde thiosemicarbazone (3-AP) using a single intravenous dose schedule. Cancer Chemother Pharmacol. 2002; 50: 223–9. https://doi.org/10.1007/s00280-002-0480-0 PMID: 12203104
6. Mackenzie MJ, Saltman D, Hirte H, Low J, Johnson C, Pond G, et al. A Phase II study of 3-aminopyridine-2-carboxaldehyde thiosemicarbazone (3-AP) and gemcitabine in advanced pancreatic carcinoma. A trial of the Princess Margaret hospital Phase II consortium. Invest New Drugs. 2007; 25: 553–8. https://doi.org/10.1007/s10637-007-9066-3 PMID: 17585372
7. Chao J, Synold TW, Morgan RJ, Kunos C, Longmate J, Lenz H-J, et al. A phase I and pharmacokinetic study of oral 3-aminopyridine-2-carboxaldehyde thiosemicarbazone (3-AP, NSC #663249) in the treatment of advanced-stage solid cancers: a California Cancer Consortium Study. Cancer Chemother Pharmacol. 2012; 69: 835–43. https://doi.org/10.1007/s00280-011-1779-5 PMID: 22105720
8. Odenike OM, Larson RA, Gajria D, Dolan ME, Delaney SM, Karrison TG, et al. Phase I study of the ribonucleotide reductase inhibitor 3-aminopyridine-2-carboxaldehyde-thiosemicarbazone (3-AP) in combination with high dose cytarabine in patients with advanced myeloid leukemia. Invest New Drugs. 2008; 26: 233–9. https://doi.org/10.1007/s10637-008-9115-6 PMID: 18217206
9. Yen Y, Margolin K, Doroshow J, Fishman M, Johnson B, Clairmont C, et al. A phase I trial of 3-aminopyridine-2-carboxaldehyde thiosemicarbazone in combination with gemcitabine for patients with advanced cancer. Cancer Chemother Pharmacol. 2004; 54: 331–42. https://doi.org/10.1007/s00280-004-0821-2 PMID: 15148626
10. Liu MC, Lin TS, Sartorelli AC. Synthesis and Antitumor Activity of Amino Derivatives of Pyridine-2-carboxaldehyde Thiosemicarbazone. J Med Chem. 1992; 35: 3672–3677. PMID: 1433178
11. Giles FJ, Fracasso PM, Kantarjian HM, Cortes JE, Brown RA, Verstovsek S, et al. Phase I and pharmacodynamic study of Triapine, a novel ribonucleotide reductase inhibitor, in patients with advanced leukemia. Leuk Res. 2003; 27: 1077–83. PMID: 12921943
12. Attia S, Kolesar J, Mahoney MR, Pitot HC, Laheru D, Heun J, et al. A phase 2 consortium (P2C) trial of 3-aminopyridine-2-carboxaldehyde thiosemicarbazone (3-AP) for advanced adenocarcinoma of the pancreas. Invest New Drugs. 2008; 26: 369–79. https://doi.org/10.1007/s10637-008-9123-6 PMID: 18278438
13. Knox JJ, Hotte SJ, Kollmannsberger C, Winquist E, Fisher B, Eisenhauer EA. Phase II study of Triapine in patients with metastatic renal cell carcinoma: a trial of the National Cancer Institute of Canada Clinical

Trials Group (NCIC IND.161). Invest New Drugs. 2007; 25: 471–7. https://doi.org/10.1007/s10637-007-9044-9 PMID: 17393073

14. Kowol CR, Trondl R, Heffeter P, Arion VB, Jakupec MA, Roller A, et al. Impact of metal coordination on cytotoxicity of 3-aminopyridine-2- carboxaldehyde thiosemicarbazone (Triapine) and novel insights into terminal dimethylation. J Med Chem. 2009; 52: 5032–5043. https://doi.org/10.1021/jm900528d PMID: 19637923
15. Easmon J, Pürstinger G, Heinisch G, Roth T, Fiebig HH, Holzer W, et al. Synthesis, cytotoxicity, and antitumor activity of copper(II) and iron(II) complexes of (4)N-azabicyclo[3.2.2]nonane thiosemicarbazones derived from acyl diazines. J Med Chem. 2001; 44: 2164–71. PMID: 11405653
16. Yu Y, Kalinowski DS, Kovacevic Z, Siafakas AR, Jansson PJ, Stefani C, et al. Thiosemicarbazones from the old to new: iron chelators that are more than just ribonucleotide reductase inhibitors. J Med Chem. 2009; 52: 5271–94. https://doi.org/10.1021/jm900552r PMID: 19601577
17. Aye Y, Long MJC, Stubbe J. Mechanistic studies of semicarbazone triapine targeting human ribonucleotide reductase in vitro and in mammalian cells: Tyrosyl radical quenching not involving reactive oxygen species. J Biol Chem. 2012; 287: 35768–35778. https://doi.org/10.1074/jbc.M112.396911 PMID: 22915594
18. Evans RW, Kong X, Hider RC. Iron mobilization from transferrin by therapeutic iron chelating agents. Biochim Biophys Acta. 2012; 1820: 282–290. https://doi.org/10.1016/j.bbagen.2011.11.007 PMID: 22155077
19. Thelander L, Gräslund A, Thelander M. Continual presence of oxygen and iron required for mammalian ribonucleotide reduction: possible regulation mechanism. Biochem Biophys Res Commun. 1983; 110: 859–65. PMID: 6340669
20. Kalinowski D, Richardson D. The evolution of iron chelators for the treatment of iron overload disease and cancer. Pharmacol Rev. 2005; 57: 547–583. https://doi.org/10.1124/pr.57.4.2 PMID: 16382108
21. Serda M, Kalinowski DS, Rasko N, Potůčková E, Mrozek-Wilczkiewicz A, Musiol R, et al. Exploring the Anti-Cancer Activity of Novel Thiosemicarbazones Generated through the Combination of Retro-Fragments: Dissection of Critical Structure-Activity Relationships. PLoS One. 2014; 9: e110291. https://doi.org/10.1371/journal.pone.0110291 PMID: 25329549
22. Hu W, Zhou W, Xia C, Wen X. Synthesis and anticancer activity of thiosemicarbazones. Bioorg Med Chem Lett. 2006; 16: 2213–8. https://doi.org/10.1016/j.bmcl.2006.01.048 PMID: 16458509
23. Stanojkovic TP, Kovala-Demertzi D, Primikyri A, Garcia-Santos I, Castineiras A, Juranic Z, et al. Zinc(II) complexes of 2-acetyl pyridine 1-(4-fluorophenyl)-piperazinyl thiosemicarbazone: Synthesis, spectroscopic study and crystal structures—potential anticancer drugs. J Inorg Biochem. 2010; 104: 467–76. https://doi.org/10.1016/j.jinorgbio.2009.12.021 PMID: 20102782
24. Faist J, Seebacher W, Saf R, Brun R, Kaiser M, Weis R. New N-methylpiperazinyl derivatives of bicyclic antiprotozoal compounds. Eur J Med Chem. 2012; 47: 510–9. https://doi.org/10.1016/j.ejmech.2011.11.022 PMID: 22136906
25. Ochi T, Sakamoto M, Minamida A, Suzuki K, Ueda T, Une T, et al. Syntheses and properties of the major hydroxy metabolites in humans of blonanserin AD-5423, a novel antipsychotic agent. Bioorg Med Chem Lett. 2005; 15: 1055–9. https://doi.org/10.1016/j.bmcl.2004.12.028 PMID: 15686911
26. Schiller DS, Fung HB. Posaconazole: an extended-spectrum triazole antifungal agent. Clin Ther. 2007; 29: 1862–86. https://doi.org/10.1016/j.clinthera.2007.09.015 PMID: 18035188
27. Ae N, Fujiwara Y. Process of a quaternary ammonium salt. US20110263847A1, 2011.
28. Rathi AK, Syed R, Shin H-S, Patel R V. Piperazine derivatives for therapeutic use: a patent review (2010-present). Expert Opin Ther Pat. 2016; 26: 777–97. https://doi.org/10.1080/13543776.2016.1189902 PMID: 27177234
29. Tarushi A, Polatoglou E, Kljun J, Turel I, Psomas G, Kessissoglou DP. Interaction of Zn(II) with quinolone drugs: structure and biological evaluation. Dalton Trans. 2011; 40: 9461–73. https://doi.org/10.1039/c1dt10870k PMID: 21853189
30. Kubícek V, Havlícková J, Kotek J, Tircsó G, Hermann P, Tóth E, et al. Gallium(III) complexes of DOTA and DOTA-monoamide: kinetic and thermodynamic studies. Inorg Chem. 2010; 49: 10960–9. https://doi.org/10.1021/ic101378s PMID: 21047078
31. Proschak E, Tanrikulu Y, Schneider G. Chapter 7: Fragment-based de novo design of drug-like molecules. In: Varnek A, Tropsha A, editors. Chemoinformatics approaches to virtual screening. Cambridge: Royal Society Press; 2008. pp. 217–239.
32. Lovejoy DB, Sharp DM, Seebacher N, Obeidy P, Prichard T, Stefani C, et al. Novel second-generation di-2-pyridylketone thiosemicarbazones show synergism with standard chemotherapeutics and demonstrate potent activity against lung cancer xenografts after oral and intravenous administration in vivo. J Med Chem. 2012; 55: 7230–44. https://doi.org/10.1021/jm300768u PMID: 22861499

33. Richardson DR, Sharpe PC, Lovejoy DB, Senaratne D, Kalinowski DS, Islam M, et al. Dipyridyl thiosemicarbazone chelators with potent and selective antitumor activity form iron complexes with redox activity. J Med Chem. 2006; 49: 6510–21. https://doi.org/10.1021/jm0606342 PMID: 17064069

34. Yuan J, Lovejoy DB, Richardson DR. Novel di-2-pyridyl–derived iron chelators with marked and selective antitumor activity: in vitro and in vivo assessment. Blood. 2004; 104: 1450–1458. https://doi.org/10.1182/blood-2004-03-0868 PMID: 15150082

35. Becker EM, Lovejoy DB, Greer JM, Watts R, Richardson DR. Identification of the di-pyridyl ketone isonicotinoyl hydrazone (PKIH) analogues as potent iron chelators and anti-tumour agents. Br J Pharmacol. 2003; 138: 819–30. https://doi.org/10.1038/sj.bjp.0705089 PMID: 12642383

36. Wang Y, Ai J, Wang Y, Chen Y, Wang L, Liu G, et al. Synthesis and c-Met kinase inhibition of 3,5-disubstituted and 3,5,7-trisubstituted quinolines: identification of 3-(4-acetylpiperazin-1-yl)-5-(3-nitrobenzylamino)-7- (trifluoromethyl)quinoline as a novel anticancer agent. J Med Chem. 2011; 54: 2127–42. https://doi.org/10.1021/jm101340q PMID: 21405128

37. Hu L, Cao T, Lv Y, Ding Y, Yang L, Zhang Q, et al. Design, synthesis, and biological activity of 4-(imidazo[1,2-b]pyridazin-3-yl)-1H-pyrazol-1-yl-phenylbenzamide derivatives as BCR–ABL kinase inhibitors. Bioorg Med Chem Lett. 2016; 26: 5830–5835. https://doi.org/10.1016/j.bmcl.2016.10.007 PMID: 28029512

38. Hou X, Ge Z, Wang T, Guo W, Cui J, Cheng T, et al. Dithiocarbamic acid esters as anticancer agent. Part 1: 4-Substituted-piperazine-1-carbodithioic acid 3-cyano-3,3-diphenyl-propyl esters. Bioorg Med Chem Lett. 2006; 16: 4214–4219. https://doi.org/10.1016/j.bmcl.2006.05.085 PMID: 16766185

39. Yu K, Toral-Barza L, Shi C, Zhang W-G, Lucas J, Shor B, et al. Biochemical, cellular, and in vivo activity of novel ATP-competitive and selective inhibitors of the mammalian target of rapamycin. Cancer Res. 2009; 69: 6232–40. https://doi.org/10.1158/0008-5472.CAN-09-0299 PMID: 19584280

40. Gao H, Yamasaki EF, Chan KK, Shen LL, Snapka RM. DNA sequence specificity for topoisomerase II poisoning by the quinoxaline anticancer drugs XK469 and CQS. Mol Pharmacol. 2003; 63: 1382–8. https://doi.org/10.1124/mol.63.6.1382 PMID: 12761349

41. Serda M, Kalinowski DS, Mrozek-Wilczkiewicz A, Musiol R, Szurko A, Ratuszna A, et al. Synthesis and Characterization of Quinoline-Based Thiosemicarbazones and Correlation of Cellular Iron-Binding Efficacy to Anti-Tumor Efficacy. Bioorg Med Chem Lett. 2012; 22: 5527–5531. https://doi.org/10.1016/j.bmcl.2012.07.030 PMID: 22858101

42. Mrozek-Wilczkiewicz A, Serda M, Musiol R, Malecki G, Szurko A, Muchowicz A, et al. Iron Chelators in Photodynamic Therapy Revisited: Synergistic Effect by Novel Highly Active Thiosemicarbazones. ACS Med Chem Lett. 2014; 5: 336–339. https://doi.org/10.1021/ml400422a PMID: 24900837

43. Ghose AK, Crippen GM. Atomic physicochemical parameters for three-dimensional-structure-directed quantitative structure-activity relationships. 2. Modeling dispersive and hydrophobic interactions. J Chem Inf Comput Sci. 1987; 27: 21–35. PMID: 3558506

44. Kalinowski DS, Richardson DR. The evolution of iron chelators for the treatment of iron overload disease and cancer. Pharmacol Rev. 2005; 57: 547–83. https://doi.org/10.1124/pr.57.4.2 PMID: 16382108

45. Enyedy ÉA, Nagy N V., Zsigó É, Kowol CR, Arion VB, Keppler BK, et al. Comparative Solution Equilibrium Study of the Interactions of Copper(II), Iron(II) and Zinc(II) with Triapine (3-Aminopyridine-2-carbaldehyde Thiosemicarbazone) and Related Ligands. Eur J Inorg Chem. 2010; 2010: 1717–1728.

46. Enyedy ÉA, Zsigó É, Nagy N V., Kowol CR, Roller A, Keppler BK, et al. Complex-Formation Ability of Salicylaldehyde Thiosemicarbazone towards Zn II, Cu II, Fe II, Fe III and Ga III Ions. Eur J Inorg Chem. 2012; 2012: 4036–4047.

47. Bacher F, Dömötör O, Chugunova A, Nagy N V., Filipović L, Radulović S, et al. Strong effect of copper (II) coordination on antiproliferative activity of thiosemicarbazone-piperazine and thiosemicarbazone-morpholine hybrids. Dalt Trans. 2015; 44: 9071–9090.

48. Attwood D, Natarajan R. Effect of pH on the micellar properties of amphiphilic drugs in aqueous solution. J Pharm Pharmacol. 1981; 33: 136–140. PMID: 6116752

49. Lacivita E, Leopoldo M, Giorgio P De, Berardi F, Perrone R. Determination of 1-aryl-4-propylpiperazine pKa values: The substituent on aryl modulates basicity. Bioorg Med Chem. 2009; 17: 1339–1344. https://doi.org/10.1016/j.bmc.2008.12.015 PMID: 19121584

50. Smyth M., Smyth WF, Palmer R., Clifford J. Acid—base equilibria of some benzhydryl piperazine derivatives. Anal Chim Acta. 1976; 86: 185–194.

51. Enyedy ÉA, Primik MF, Kowol CR, Arion VB, Kiss T, Keppler BK. Interaction of Triapine and related thiosemicarbazones with iron(III)/(II) and gallium(III): a comparative solution equilibrium study. Dalton Trans. 2011; 40: 5895–905. https://doi.org/10.1039/c0dt01835j PMID: 21523301

52. Perrin DD, Dempsey B, Serjeant EP. pK a Prediction for Organic Acids and Bases [Internet]. Dordrecht: Springer Netherlands; 1981.

53. Beck MT, Nagypal I. Chemistry of Complex Equilibria. Williams DR, editor. Ellis Horwood; New York: Halsted; 1990.

54. Richardson DR, Wis Vitolo LM, Hefter GT, May PM, Clare BW, Webb J, et al. Iron chelators of the pyridoxal isonicotinoyl hydrazone class Part I. Ionisation characteristics of the ligands and their relevance to biological properties. Inorganica Chim Acta. 1990; 170: 165–170.

55. Xie W, Xie S, Zhou Y, Tang X, Liu J, Yang W, et al. Design and synthesis of novel 5,6-disubstituted pyridine-2,3-dione-3-thiosemicarbazone derivatives as potential anticancer agents. Eur J Med Chem. 2014; 81: 22–7. https://doi.org/10.1016/j.ejmech.2014.05.001 PMID: 24819956

56. Serda M, Mrozek-Wilczkiewicz A, Jampilek J, Pesko M, Kralova K, Vejsova M, et al. Investigation of the Biological Properties of (Hetero)Aromatic Thiosemicarbazones. Molecules. 2012; 17: 13483–13502. https://doi.org/10.3390/molecules171113483 PMID: 23151918

57. Serda M, Małecki JG, Mrozek-Wilczkiewicz A, Musioł R, Polański J. Microwave assisted synthesis, X-ray crystallography and DFT calculations of selected aromatic thiosemicarbazones. J Mol Struct. 2013; 1037: 63–72.

58. Sestak V, Stariat J, Cermanova J, Potuckova E, Chladek J, Roh J, et al. Novel and potent anti-tumor and anti-metastatic di-2-pyridylketone thiosemicarbazones demonstrate marked differences in pharmacology between the first and second generation lead agents. Oncotarget. 2015; 6: 42411–42428. https://doi.org/10.18632/oncotarget.6389 PMID: 26623727

59. Siegers CP, Bumann D, Trepkau HD, Schadwinkel B, Baretton G. Influence of dietary iron overload on cell proliferation and intestinal tumorigenesis in mice. Cancer Lett. 1992; 65: 245–9. PMID: 1516040

60. Chaston TB, Richardson DR. Iron chelators for the treatment of iron overload disease: relationship between structure, redox activity, and toxicity. Am J Hematol. 2003; 73: 200–10. https://doi.org/10.1002/ajh.10348 PMID: 12827659

61. Chekhun VF, Lukyanova NY, Burlaka CACP, Bezdenezhnykh NA, Shpyleva SI, Tryndyak VP, et al. Iron metabolism disturbances in the MCF-7 human breast cancer cells with acquired resistance to doxorubicin and cisplatin. Int J Oncol. 2013; 43: 1481–6. https://doi.org/10.3892/ijo.2013.2063 PMID: 23969999

62. Miller LD, Coffman LG, Chou JW, Black MA, Bergh J, D'Agostino R, et al. An iron regulatory gene signature predicts outcome in breast cancer. Cancer Res. 2011; 71: 6728–6737. https://doi.org/10.1158/0008-5472.CAN-11-1870 PMID: 21875943

63. Torti S V, Torti FM. Cellular iron metabolism in prognosis and therapy of breast cancer. Crit Rev Oncog. 2013; 18: 435–48. PMID: 23879588

64. Pinnix ZK, Miller LD, Wang W, D'Agostino R, Kute T, Willingham MC, et al. Ferroportin and iron regulation in breast cancer progression and prognosis. Sci Transl Med. 2010; 2: 43ra56. https://doi.org/10.1126/scisignal.3001127 PMID: 20686179

65. Omuro A, DeAngelis LM. Glioblastoma and other malignant gliomas: a clinical review. JAMA. 2013; 310: 1842–50. https://doi.org/10.1001/jama.2013.280319 PMID: 24193082

66. Louis DN, Ohgaki H, Wiestler OD, Cavenee WK, Burger PC, Jouvet A, et al. The 2007 WHO classification of tumours of the central nervous system. Acta Neuropathol. 2007; 114: 97–109. https://doi.org/10.1007/s00401-007-0243-4 PMID: 17618441

67. Legendre C, Garcion E. Iron metabolism: A double-edged sword in the resistance of glioblastoma to therapies. Trends Endocrinol Metab. Elsevier Ltd; 2015; 26: 322–331. https://doi.org/10.1016/j.tem.2015.03.008 PMID: 25936466

68. Legendre C, Avril S, Guillet C, Garcion E. Low oxygen tension reverses antineoplastic effect of iron chelator deferasirox in human glioblastoma cells. BMC Cancer. BMC Cancer; 2016; 16: 51. https://doi.org/10.1186/s12885-016-2074-y PMID: 26832741

69. Gosselaar PH, Van-Dijk AJG, De-Gast GC, Polito L, Bolognesi A, Vooijs WC, et al. Transferrin toxin but not transferrin receptor immunotoxin is influenced by free transferrin and iron saturation. Eur J Clin Invest. 2002; 32 Suppl 1: 61–9.

70. Lee JC, Chiang KC, Feng TH, Chen YJ, Chuang ST, Tsui KH, et al. The Iron Chelator, Dp44mT, Effectively Inhibits Human Oral Squamous Cell Carcinoma Cell Growth in Vitro and in Vivo. Int J Mol Sci. 2016; 17: 1–13.

71. Le NTV, Richardson DR. Iron chelators with high antiproliferative activity up-regulate the expression of a growth inhibitory and metastasis suppressor gene: a link between iron metabolism and proliferation. Blood. 2004; 104: 2967–2975. https://doi.org/10.1182/blood-2004-05-1866 PMID: 15251988

72. Shen J, Sheng X, Chang Z, Wu Q, Wang S, Xuan Z, et al. Iron metabolism regulates p53 signaling through direct Heme-p53 interaction and modulation of p53 localization, stability, and function. Cell Rep. 2014; 7: 180–193. https://doi.org/10.1016/j.celrep.2014.02.042 PMID: 24685134

73. Le N. The role of iron in cell cycle progression and the proliferation of neoplastic cells. Biochim Biophys Acta—Rev Cancer. 2002; 1603: 31–46.

74. Yu Y, Kovacevic Z, Richardson DR. Tuning cell cycle regulation with an iron key. Cell Cycle. 2007; 6: 1982–1994. https://doi.org/10.4161/cc.6.16.4603 PMID: 17721086

75. Cheng M, Olivier P, Diehl JA, Fero M, Roussel MF, Roberts JM, et al. The p21(Cip1) and p27(Kip1) CDK "inhibitors" are essential activators of cyclin D-dependent kinases in murine fibroblasts. EMBO J. 1999; 18: 1571–83. https://doi.org/10.1093/emboj/18.6.1571 PMID: 10075928

76. Yu Y, Rahmanto YS, Richardson DR. Bp44mT: An orally active iron chelator of the thiosemicarbazone class with potent anti-tumour efficacy. Br J Pharmacol. Wiley-Blackwell; 2012; 165: 148–166. https://doi.org/10.1111/j.1476-5381.2011.01526.x PMID: 21658021

77. Kovacevic Z, Chikhani S. Novel thiosemicarbazone iron chelators induce up-regulation and phosphorylation of the metastasis suppressor N-myc down-stream regulated gene 1: a new strategy. Mol Pharmacol. 2011; 80: 598–609. https://doi.org/10.1124/mol.111.073627 PMID: 21719465

78. McIlwain DR, Berger T, Mak TW. Caspase Functions in Cell Death and Disease. Cold Spring Harb Perspect Biol. 2013; 5: a008656–a008656. https://doi.org/10.1101/cshperspect.a008656 PMID: 23545416

79. Elmore S. Apoptosis: a review of programmed cell death. Toxicol Pathol. 2007; 35: 495–516. https://doi.org/10.1080/01926230701320337 PMID: 17562483

80. Liang Y, Yan C, Schor NF. Apoptosis in the absence of caspase 3. Oncogene. 2001; 20: 6570–6578. https://doi.org/10.1038/sj.onc.1204815 PMID: 11641782

81. Gomez-Manzano C, Fueyo J, Kyritsis AP, Steck PA, Levin VA, Alfred Yung WK, et al. Characterization of p53 and p21 Functional Interactions in Glioma Cells en Route to Apoptosis. JNCI J Natl Cancer Inst. 1997; 89: 1036–1044. PMID: 9230885

82. Brázdová M, Quante T, Tögel L, Walter K, Loscher C, Tichý V, et al. Modulation of gene expression in U251 glioblastoma cells by binding of mutant p53 R273H to intronic and intergenic sequences. Nucleic Acids Res. 2009; 37: 1486–1500. https://doi.org/10.1093/nar/gkn1085 PMID: 19139068

83. Gans P, Sabatini A, Vacca A. Hypspec 2000. Leeds UK, Florence Italy;

84. Alderighi L, Gans P, Ienco A, Peters D, Sabatini A, Vacca A. Hyperquad simulation and speciation (HySS): a utility program for the investigation of equilibria involving soluble and partially soluble species. Coord Chem Rev. 1999; 184: 311–318.